Reactive Molecular Dynamics: From Small Molecules to Proteins

Markus Meuwly*

Article Type:

Advanced Review

Abstract

The current status of reactive molecular dynamics (MD) simulations is summarized. Both, methodological aspects and applications to problems ranging from gas phase reaction dynamics to ligand-binding in solvated proteins are discussed, focusing on extracting information from simulations that can not easily be obtained from experiments alone. One specific example is the structural interpretation of the ligand rebinding time scales extracted from state-of-the art time resolved experiments. Atomistic simulations employing validated reactive interaction potentials are capable of providing structural information about the time scales involved. Both, merits and shortcomings of the various methods are discussed and the outlook summarizes possible future avenues such as reactive potentials based on machine learning techniques.

---

*Department of Chemistry, University of Basel, Basel, Switzerland and Department of Chemistry, Brown University, Providence, RI, USA

GRAPHICAL TABLE OF CONTENTS

INTRODUCTION

Understanding atomistic and molecular details of chemical reactions is one of the corner-stones in chemistry and biology. Characterizing reactions in time and space is challenging because the nuclear motion on various length- and time-scales needs to be followed.(El Hage et al., 2017) As an example, typical reaction times in the Claisen rearrangement(Claisen, 1912) are on the order of seconds (in aqueous solution)(Andrews, Smith, & Young, 1973) or milliseconds (in the protein).(Kast, Asif-Ullah, & Hilvert, 1996) However, the actual chemical step (i.e. C-C bond formation and C-O bond breaking) occurs on the femtosecond time scale. In other words, during 10^9 to 10^{15} vibrational periods energy is redistributed in the system until sufficient energy has accumulated along the preferred "progression coordinate" for the reaction to occur. Because the "chemical step" is so rapid and the concentration of systems at the transition state is tiny, direct experimental characterization of a chemical reaction between reactant, transition state and product is extremely challenging even with current state-of-the art methods, including NMR,(D. Li, Keresztes, Hopson, & Williard, 2009) IR,(Helbing et al., 2004) or X-ray(Schotte et al., 2003; Kern et al., 2014) spectroscopic techniques or combinations thereof.

Atomistic simulations have shown their value in providing molecular-level insights into the energetics and dynamics of chemical reactions for systems ranging from small (triatomic) molecules to proteins in the condensed phase. An essential requirement for a meaningful contribution of computer-based work to understand and characterize chemical reactions is the quantitatively correct description of the intermolecular interactions along the entire reaction path. This involves regions around the reactants, products and the transition state(s). Intermolecular interactions in molecular systems are often represented as Born-Oppenheimer potential energy surfaces (BO-PESs or PESs). As such, these are $3N - 6$ dimensional hypersurfaces, where N is the number of atoms. This already makes clear that a realistic representation of this object $V(\vec{x})$, where $\vec{x}$ is a $3N$ dimensional vector con-

taining all Cartesian coordinates, is a formidable undertaking. Following the dynamics on the PES is either done based on Newtonian mechanics(Brooks et al., 2009; Hess, Kutzner, van der Spoel, & Lindahl, 2008) ("molecular dynamics simulations") or by solving the time-independent(Skouteris, Castillo, & Manolopoulos, 2000) or time-dependent(Peng, Zhang, Wang, Li, & Zhang, 2000; Mayneris, Gonzalez, & Gray, 2008) Schrödinger equation for a quantum mechanical approach. In recent years, path-integral-based approaches and variants thereof(Beyer, Richardson, Knowles, Rommel, & Althorpe, 2016) have also been explored.

Broadly speaking, there are two possible approaches for following chemical reactions using molecular dynamics (MD) simulations: those using quantum mechanics (QM)-based methods and those employing empirical force fields. Empirical energy functions represent the PES in one way or another as a computable function (see below) whereas QM-based methods solve the electronic Schrödinger equation directly for every configuration $\vec{x}$ of the system for which it is required, for a review see Ref.(Cui, 2016) This is a very powerful technique as it provides a general framework for investigating the dynamics of chemical reactivity without preconceived reaction mechanisms. However, there are certain limitations which are due to the computational approach *per se* (such as the speed and efficiency of the method) or due to practical aspects of quantum chemistry (e.g. basis set superposition error, the convergence of the Hartree-Fock wavefunction to the desired electronic state for arbitrary geometries, or the choice of a suitable active space irrespective of molecular geometry). Improvements and future avenues for making QM-based approaches even more broadly applicable have been recently discussed.(Cui, 2016)

A particularly promising use of QM-based methods are mixed quantum mechanics/molecular mechanics (QM/MM) treatments which are popular for biophysical and biochemical applications.(Senn & Thiel, 2009) Using a decomposition into a "reactive region" which is treated with a quantum chemical (or semiempirical) method and an environment described by an empirical force field can considerably speed up simulations such that even free energy simulations in multiple dimensions can be computed.(Roston, Demapan, & Cui, 2016) One of the current open questions in such QM/MM simulations is that of the size of the QM region required for

converged results which was recently considered for Catechol O-Methyltransferase.(Kulik, Zhang, Klinman, & Martinez, 2016)

The focus of the present review is on the use of empirical energy functions to follow chemical reactions in the gas- and condensed phase. The motivation for this is twofold: first, due to their computational efficiency formulations based on empirical energy functions are expected to be suitable for situations where extensive sampling of the conformational space is required. Secondly, force fields fitted to electronic structure data, experimental observables or both can be systematically improved. However, most of the available approaches are not unbiased as they have to make assumptions about the bonding pattern for the states involved in the chemical transformation considered. In the following, several techniques to investigate chemical reactivity suitable for exploration through MD simulations are presented. This is done by adopting a historical perspective to highlight how the field has developed. Next, topical examples are discussed with a particular focus on relating the reactive dynamics with the time scales of elementary processes and the underlying conformational dynamics.

Computational Techniques

Already in the 50s Linus Pauling - based on earlier work by Penney(Penney, 1937) - suggested that bond order and bond length are related.(Pauling, 1947) It was also recognized that the (fractional) bond order is related to the strength of the bond considered, i.e. to the interaction energy.(Penney, 1937) Following this, Johnston and Parr proposed a "bond energy bond order" (BEBO) potential.(Johnston & Parr, 1963) It was found that a) there exists a nearly linear relationship between bond order and bond length (Pauling, 1947) and b) a log-log plot of dissociation energies versus bond order is also almost linear. This approach yielded activation energies within ≈ 2 kcal/mol and chemical rates within an order of magnitude for well-known bond energies. One of the essential assumptions underlying this approach is that - at least for hydrogen-atom transfer reactions - the sum of the bond orders n_1 of the breaking and the newly formed bond n_2 fulfills $n_1 + n_2 = 1$. In other words: "At

all stages of the reaction the formation of the second bond must be 'paying for' the breaking of the first bond".(Johnston & Parr, 1963)

ReaxFF

An extension of the concept (and observation) that bond order, bond length and bond energy are related is the ReaxFF force field.(van Duin, Dasgupta, Lorant, & Goddard III, 2001) Here, van der Waals and Coulomb terms are included at the outset of the development and the dissociation and reaction curves are derived from electronic structure calculations. The total energy in ReaxFF is(van Duin et al., 2001; Chenoweth, van Duin, & Goddard, 2008)

$$E = E_{\mathrm{bond}} + E_{\mathrm{over}} + E_{\mathrm{under}} + E_{\mathrm{conj}} + E_{\mathrm{val}} + E_{\mathrm{pen}} + E_{\mathrm{dihe}} + E_{\mathrm{VdW}} + E_{\mathrm{coul}} \tag{1}$$

Here, $E_{\mathrm{val}}, E_{\mathrm{dihe}}, E_{\mathrm{VdW}}$ and E_{coul} are the well-known valence-angle, dihedral, Van der Waals, and electrostatic terms. Central to ReaxFF is that the bond order can be calculated from the distance between two atoms. For a CC-bond this expresses the fact that two carbon atoms can be found to form anything between "no bond" (bond order = 0) to a triple bond. The energy term E_{bond} in the force field is calculated from the value of the bond order. To correct for over-coordination, a penalty term E_{over} is added to ReaxFF and for under-coordinated atoms additional favorable energy terms E_{under} reflecting resonance energies between $\pi-$electrons are introduced. The conjugation energy E_{conj} changes between a maximum value if successive bonds have bond-order values of 1.5 (e.g. benzene) to zero. Finally, E_{pen} reproduces the stability of systems with two double bonds sharing an atom in a valence angle. A recent review discusses the current status and future directions.(Senftle et al., 2016).

ReaxFF has been applied to a wide array of reactive chemical systems, including hydrocarbons(van Duin et al., 2001), the thermal decomposition of a zinc-oxide nanowire.(Russo & van Duin, 2011), shock-induced chemistry in high energy materials (Strachan, van Duin, Chakraborty, Dasgupta, & Goddard III, 2003), the activation and dissociation of H_2 on platinum surfaces (Ludwig, Vlachos, van Duin, & Goddard III, 2006) or the oxidation of nanoparticles on aluminum surfaces (Vashishta, Kalia, & Nakano, 2006). Using ReaxFF and nonequilibrium

MD simulations it was found that depending on the impact velocities cyclic-$[CH_2N(NO_2)]_3$ decomposes into a variety of small molecules on the picosecond time scale or only into NO_2, both of which are consistent with experiments (Strachan et al., 2003). Such simulations provide valuable insight into the time dependence of concentration changes of particular species. As such they can complement studies such as the "nanoreactor"(Wang et al., 2014) which follows a similar logic - namely characterizing the time-dependent concentration of species given a particular initial distribution of reactants and corresponding thermodynamic conditions.

Contrary to empirical force field-based methods (see below), ReaxFF does not build on the concept of atom types. While the functional form of ReaxFF is universal, its application to concrete problems always involves more or less extensive fitting to reference calculations.(Senftle et al., 2016) Also, with respect to actual parametrizations, it is noted that several "branches" exist (e.g. the aqueous or combustion branch). The parametrizations for one chemical element in two different branches do not necessarily transfer.(Senftle et al., 2016)

Empirical Valence Bond

A natural starting point to formulate a model for chemical reactivity in complex environments (e.g. in solution or a protein) is valence bond theory. This has been done within the framework of the empirical valence bond (EVB) approach.(Duarte & Kamerlin, 2017) As noted in the original EVB publication "The user[..] must choose, on the basis of experience and intuition, a set of bonding arrangements or "resonance structures"[..]".(Warshel & Weiss, 1980; Hong, Rosta, & Warshel, 2006). Since the reactive species and its environment primarily interact through electrostatic interactions, empirical force fields can be used to describe the resonant forms of the reactant and product states. For ionic bond cleavage AB→A$^-$+B$^+$, three resonance forms are considered: $\psi_1 = AB$, $\psi_2 = A^-B^+$, and $\psi_3 = A^+B^-$.(Warshel & Weiss, 1980) If A is more electronegative than B (i.e. formation B$^-$ is unlikely in the presence of A), resonance structure ψ_3 is largely irrelevant and the process

can be described by ψ_1 and ψ_2 alone. The choice of the necessary states in EVB is not always obvious *a priori* but may also need to be based, e.g., on the requirement to best reproduce the reference electronic structure calculations.(Glowacki, Orr-Ewing, & Harvey, 2015)

For a collection of covalent and ionic states, matrix elements for the EVB Hamiltonian have to be determined. They include diagonal elements H_{ii} for the covalent and ionic states, and off-diagonal elements that couple configurations (bonding patterns) that differ by the location of an electron pair. All other off-diagonal matrix elements H_{ij} are zero. The justification for this is that such matrix elements are proportional to the square or higher powers of the overlap between atomic orbitals, but they may also be retained (Coulson & Danielsson, 1954; Warshel & Weiss, 1980). The covalent diagonal matrix elements H_{ii} correspond essentially to an empirical force field, whereas for the ionic diagonal matrix elements the bonded terms are replaced by electrostatic interactions between the charged fragments and the formation energy of A^-B^+ from AB has also to be added. For the two-fragment system AB the matrix elements are $H_{11} = D_e(1 - \exp[-\beta(r - r_e)])^2$ and $H_{22} = \Delta - \frac{e^2}{r} + V_{nb}$ where Δ is the gas-phase formation energy of A^-B^+ from AB at infinite separation, and V_{nb} is the nonbonded interaction potential such that the minimum of $(\frac{-e^2}{r} + V_{nb})$ is given by the sums of the ionic radii of A^+ and B^-. In the original version of EVB(Warshel & Weiss, 1980) the off-diagonal element $H_{12} = H_{21}$ is determined through the requirement that the eigenvalues of the Hamiltonian E satisfy the relation $H_{12} = \sqrt{(H_{11} - E)(H_{22} - E)}$ and E is the experimentally determined ground-state bond energy. In a later and slightly more general approach, the off-diagonal elements are parametrized functions depending on a pre-defined reaction coordinate of the form $H_{ij} = A \exp(-\mu(r - r_0))$ (Hong et al., 2006), where A, μ and r_0 are fitting parameters.

The definition of the off-diagonal terms has been a source of considerable discussion, in particular the assumption that upon transfer of the reaction from the gas phase to the solution phase these elements do not change significantly.(Hong et al., 2006). Alternative forms which also capture the shape and energetics of the potential energy surface around the transition state use generalized Gaussians (Chang & Miller, 1990). A comparison of different diabatic

models provides a notion of the common features and the differences between various approaches (Valero, Song, Gao, & Truhlar, 2009b, 2009a; Kamerlin, Cao, Rosta, & Warshel, 2009). A useful comparison of the similarities and differences between the various methods can be found in Ref. (Florian, 2002). Applications of EVB include enzymatic reactions (for which it was originally developed (Warshel, 1984)), proton transfer processes, and the autodissociation of water (Strajbl, Hong, & Warshel, 2002). More recently, this has been extended to other types of reactions, including bimolecular reactions(Greaves et al., 2011; Glowacki, Rose, Greaves, Orr-Ewing, & Harvey, 2011) or the association and dissociation of CH_3 from diamond surfaces.(Glowacki, Rodgers, Shannon, Robertson, & Harvey, 2017) Furthermore, several extensions have been suggested to the original EVB method allowing its application to a wider class of problems.(Chang & Miller, 1990; Schmitt & Voth, 1998; Schlegel & Sonnenberg, 2006).

Reactive Molecular Dynamics: Mixing PESs in Time and Energy

Time resolved experiments have contributed heavily to our understanding of chemical reactivity over the past 20 years. With the advent of short laser pulses ("femtochemistry") it became possible to follow chemical transformations on the relevant time scale on which the actual chemical step (bond breaking or bond formation) occurs (see Introduction). Typical examples are the time resolved studies of ligand (re)binding in myoglobin (Mb)(Petrich et al., 1991; Nutt & Meuwly, 2006; Danielsson & Meuwly, 2008; Kruglik et al., 2010; J. Kim, Park, Lee, & Lim, 2012; Yoo, Kruglik, Lamarre, Martin, & Negrerie, 2012) or vibrationally induced reactivity.(Crim, 1993; Vaida, Kjaergaard, Hintze, & Donaldson, 2003; Y. Miller & Gerber, 2006; Yosa Reyes, Brickel, Unke, Nagy, & Meuwly, 2016; Brickel & Meuwly, 2017)

This prompted the development of computational techniques that allow following chemical reactions in time which is the natural progression coordinate in a time resolved experiment. Reactive MD(Nutt & Meuwly, 2006) was based on earlier efforts to study ligand rebinding kinetics of nitric oxide to Mb.(H. Li, Elber, & Straub, 1993; Meuwly, Becker, Stote, & Karplus, 2002) The underlying concept is to first introduce relevant "states" of the system,

i.e. bonding patterns in the language of empirical force fields. Along the MD simulation the system is then propagated on the lowest adiabatic energy $V_R(\vec{x})$ ("electronic ground state") while monitoring the energy gaps to all higher lying states for the same configuration. Once a crossing between $V_R(\vec{x})$ and any other state $V_P(\vec{x})$ higher in energy occurs the simulation is stopped, back propagated by a time t_s (half the switching time) and the two PESs involved in the crossing are mixed according to $V_{eff}(\vec{x}) = f(t)V_R(\vec{x}) + (1 - f(t))V_P(\vec{x})$ where $f(t)$ is a sigmoid switching function which changes from 1 to 0 between $t = -t_s/2$ and $t = t_2/2$. At the beginning of the mixing the system is fully in the R-state ($f(t = -t_s/s) = 1$), while at the end it is fully in the P-state ($f(t > t_s/s) = 1$). The algorithm of ARMD is schematically shown for a collinear atom transfer reaction in Figure 1a.

Time-based ARMD(Nutt & Meuwly, 2006; Danielsson & Meuwly, 2008) does not explicitly couple the PESs describing the different states considered. The only free variable is the switching time t_s over which two (or several) crossing PESs are mixed. However, no control over the crossing region is possible which may be a disadvantage of the method.

During the mixing the system is propagated under a time-dependent Hamiltonian which does not strictly conserve total energy.(Yosa & Meuwly, 2011; Nagy, Yosa Reyes, & Meuwly, 2014) The magnitude of this effect can be shown to scale with $1/m$ where m is the reduced mass involved in the reaction(Nagy et al., 2014) which is inconsequential for heavy systems such as NO rebinding to Mb but affects the dynamics in the product channel for proton transfer processes. This led to the development of multi state adiabatic reactive MD (MS-ARMD) which mixes the PESs with energy dependent weights and strictly conserves energy.(Nagy et al., 2014)

In MS-ARMD the PESs are mixed in energy-space according to

$$V_{\text{MS-ARMD}}(\vec{x}) = \sum_{i=1}^{n} w_i(\vec{x})V_i(\vec{x}) \tag{2}$$

9

Potential energy (vertical axis, panel a)

AB + C →[A⋯B⋯C]→ A + BC

3. wind back time with $t_s/2$

4. propagate on V_{ARMD} for t_s

1. propagate

2. crossing detected

B

AB Morse
A - C vdW
B - C vdW

smooth connection in TIME

BC Morse
A - B vdW
A - C vdW

5. propagate

Coordinate of atom B

(a)

Energy (panel b)

m $v_0 = v(0)$

0

$E_{kin,0}$

αx

phase II: start of ARMD switching

βx

x_0

$0 = x^I(t_s/2)$

Coordinate x

(b)
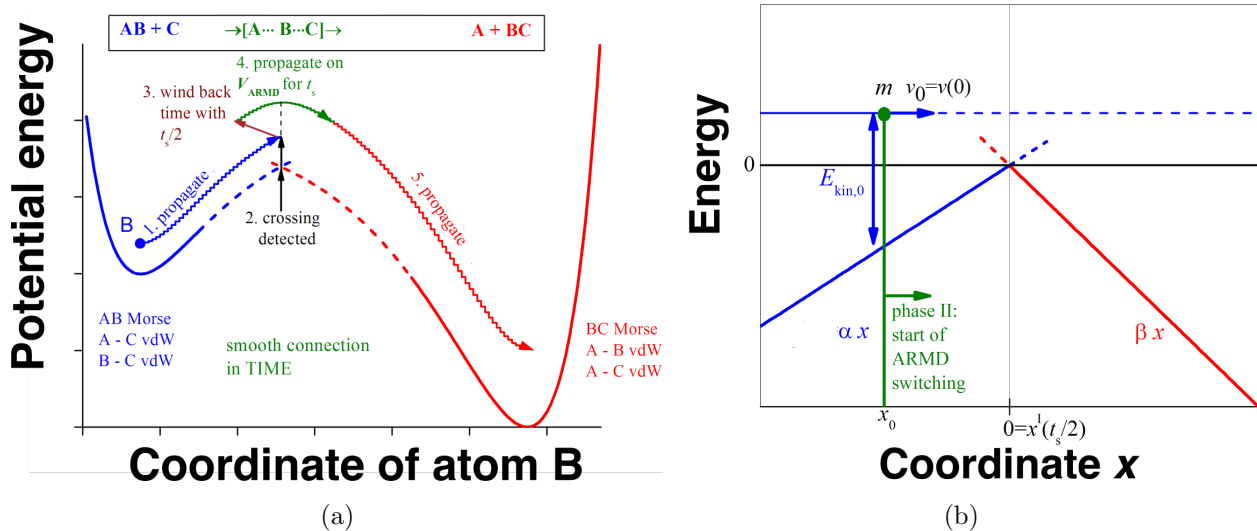
Figure 1: a) Schematic illustrating the ARMD method for a collinear reaction, where atom B is transferred from donor atom A to acceptor atom C. During crossing the surfaces are switched in time and the Morse bond is replaced by van der Waals (vdW) interactions and vice versa. b) Simple model for estimating energy violation in ARMD simulations. The system with mass m approaches from the left on PES $V_R(x) = \alpha x$ (phase I). At time $t = 0$ it is at x_0 with velocity v_0 and kinetic energy $E_{kin,0}$. After crossing is detected at $x = 0$ the time is rewound by $t_s/2$ and the dynamics is re-simulated while $V_R(x)$ is being switched to $V_P(x) = \beta x$ in t_s (phase II).

The weights (see Figure 2) $w_i(\vec{x})$ are obtained by renormalizing the raw weights $w_{i,0}(\vec{x})$

$$w_i(\vec{x}) = \frac{w_{i,0}(\vec{x})}{\sum\limits_{i=1}^{n} w_{i,0}(\vec{x})} \qquad \text{where} \quad w_{i,0}(\vec{x}) = \exp\left(-\frac{V_i(\vec{x})}{\Delta V}\right) \qquad (3)$$

The raw weights (Eq. 3) depend exponentially on the energy difference between surface i and the minimum energy surface over a characteristic energy scale ΔV (switching parameter). Only those surfaces will have significant weights, whose energy is within a few times of ΔV from the lowest energy surface. The performance of MS-ARMD is demonstrated for crossings of 1D and 2D surfaces in Figure 2. Finally, ARMD with energy-dependent weights mixes the different PESs by using Gaussian and polynomial functions (GAPOs) in the neighborhood of crossing points between the states. The parameters of these GAPOs need to be determined through fitting to reference data (e.g. from a calculation along the intrinsic reaction
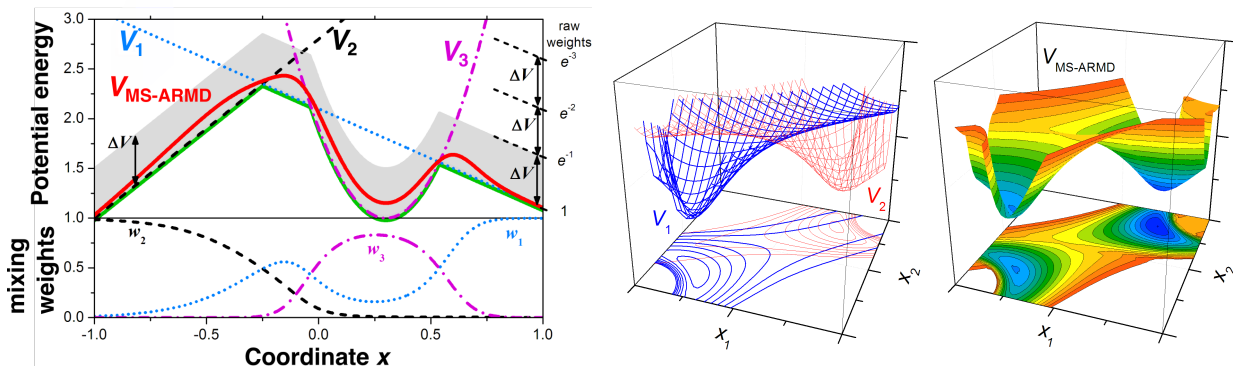
Figure 2: The MS-ARMD switching method applied in one and two dimensions to 3 and 2 surfaces ($V_{1,2,3}$). The effective surface is ($V_{\text{MS-ARMD}}$) always close to the lowest-energy surface (V_{min}), except for regions where other surfaces are within a few times ΔV (here $= 0.5$) in energy. Here, the algorithm switches smoothly among them by varying their weights ($w_{1,2,3}$; lower left panel)

coordinate (IRC)). This step is the most demanding part in MS-ARMD.(Nagy et al., 2014) A smooth global surface is obtained everywhere, even for energies where more than two surfaces approach one another. Because the mixed PES $V_{\text{MS-ARMD}}(\vec{x})$ depends on the energies of the different states through the weights w_i which in turn are analytical functions of the coordinates $\vec{x}$ the derivatives can be readily determined which leads to energy conservation in MD simulations.

A recent extension(Schmid, Das, Landis, & Meuwly, 2018) of MS-ARMD is its combination with VALBOND, a force field that allows to describe the geometries and dynamics of metal complexes.(Landis, Cleveland, & Firman, 1998; Firman & Landis, 2001; Tubert-Brohman, Schmid, & Meuwly, 2009) Here, the formulation is reminiscent of EVB whereby the diagonal terms are VALBOND descriptions of the states involved and the off-diagonal elements describe the orbital overlap. Furthermore, MS-ARMD can also be combined with molecular mechanics with proton transfer (MMPT)(Lammers, Lutz, & Meuwly, 2008) to follow proton transfer in the gas- and condensed phase.(Mackeprang, Xu, Maroun, Meuwly, & Kjaergaard, 2016; Xu & Meuwly, 2017; Karandashev, Xu, Meuwly, Vanicek, & Richardson, 2017; Xu & Meuwly, 2018)

It is instructive to briefly compare EVB and the two ARMD approaches. While all three methods start from an empirical force field perspective, the EVB constructs an $n \times n$ Hamiltonian with the force fields V_{nn} for the pure states on the diagonal and mixing elements V_{mn} ($m \neq n$) as off-diagonal elements. This Hamiltonian needs to be diagonalized at every time step of an MD simulation and the forces can be determined from the Hellmann-Feynman theorem.(Glowacki et al., 2015) The parametrization of the off-diagonal elements is the most demanding part in a concrete EVB-application. First it has to be decided, whether or not elements V_{mn} should be constants or depend on one or several explicit coordinates. If they depend on (usually internal) coordinates, one or several reaction coordinates are chosen. Such choices can sometimes be justified but determining meaningful reaction coordinates remains a challenge. The second choice is that of a functional form. Typically, exponentially decaying or Gaussian functions(Schlegel & Sonnenberg, 2006) are used. Fitting the free parameters to reference energies is the final step in this procedure.

For ARMD the challenge is to fit the Gaussian polynomials (GAPO) to describe the barrier region. Usually, the force fields for the asymptotic reactant and product states can be fitted using standard steepest descent techniques. However, for the GAPOs more advanced fitting tools are required, e.g. differential evolution.(Storn & Price, 1997) Also, as the GAPOs are formulated in "energy space" it is not straightforward to provide simple and transparent guesses for the initial parameters for the fit.

Global Potential Energy Surfaces

The most rigorous approach to reactive chemical dynamics is to use fully dimensional, reactive PESs, which are usually only available for low-dimensional systems. Specifically in the field of small molecule reactions involving processes such as A+BC→AB+C or AB+CD→A+BCD (or permutations thereof) involving a total number of 3 to 8 atoms the construction of globally valid potential energy surfaces is essential to make direct contact between computations and experiments. The limitation on up to 8 atoms is primarily owed to the fact that ac-

curately solving the nuclear Schrödinger equation for systems involving a larger number of nuclei remains an unsolved problem although considerable progress has been made over the past several years.(W. Zhang et al., 2010; Zhao, Zhang, Liu, & Zhang, 2017)

One of the earliest efforts to determine outcomes of chemical reactions is the $H+H_2$ atom exchange reaction. Using classical molecular dynamics (MD) and a modified London-Eyring-Polanyi-Sato (LEPS) surface,(Porter & Karplus, 1964) the differential cross sections for the $D+H_2$ reaction were calculated.(Karplus, Sharma, & Porter, 1964) It is of interest to note that some 10 years later the results of these quasi-classical simulations were almost quantitatively confirmed at room temperature by a full quantum treatment.(Schatz & Kuppermann, 1976) The LEPS surface(Porter & Karplus, 1964; Sato, 1955a, 1955b) was based on London's work on the $H+H_2$ reaction for which he used a 2×2 valence bond treatment (London, 1929) which is akin to an EVB-like treatment (see above). Subsequent work on fully-dimensional PESs for more complex systems further explored the use of valence bond theory and led to the diatomics-in-molecules (DIM) theory (Ellison, 1963; Olson & Garrison, 1984; Belyaev, Tiukanov, & Domcke, 2002).

A different approach was taken when determining reliable intermolecular potential energy surfaces was cast as an inversion problem from experimental - largely spectroscopic and scattering - data.(Hutson, 1990) For the special class of van der Waals complexes (AB+C, where AB is a di- or triatomic and C is a rare gas atom) the long-range part of the PES can be well described by inductive and dispersion interactions. Their functional forms are known and constrain the long-range, asymptotic region of the intermolecular interactions. For the short range part, a parametrized form was assumed (typically a damped Buckingham or a Lennard-Jones potential).(Hutson, 1990) By fitting the free parameters (usually some 10 to 20 parameters) to best reproduce the experimental observables quite accurate potential energy surfaces could be derived in this fashion for a wide range of systems, including the HF-, HCl-, and H_2-rare gas series.(LeRoy & Hutson, 1987; Hutson, 1992) However, such an "inversion scheme" is only informative about the shape of the PES in regions which are also sampled by experiment.(Meuwly & Hutson, 1999a) This "dependence" on experi-

mental data vanished when high-level (at least Moller-Plesset MP2 but better CCSD(T) or multireference-configuration interaction) electronic structure calculations became possible to provide energies for arbitrary geometries for such systems.

High-level *ab initio* calculations have become more accurate and more efficient.(White, Johnson, Gill, & Head-Gordon, 1996; Adler, Knizia, & Werner, 2007; Knizia, Adler, & Werner, 2009) Along with the ever-increasing computational power it is now possible to compute thousands of energies at various geometries for small polyatomic systems within chemical accuracy (0.5 kcal/mol).(Bokhan, Ten-No, & Noga, 2008) With the availability of routine electronic structure calculations using large basis sets and accurate ways for approximately solving the electronic Schrödinger equation the problem shifted to *representing* the computed, discrete points on the PES. This is in particular needed when running MD simulations (classical or quasiclassical trajectory (QCT) simulations) where the total energy and the derivatives at arbitrary points are required. Similarly, quantum wavepacket calculations require analytical forms of the PES whereas for collocation methods it is sometimes sufficient to work with a discrete, precomputed set of energies. Nevertheless, it is nowadays standard to represent nonreactive and reactive PESs in a manner that allows to evaluate it at arbitrary points, given pointwise information from *ab initio* calculations only. In addition, the final representation should be computationally efficient in order to run statistically significant numbers of (reactive) trajectories in QCT simulations.(Yosa & Meuwly, 2011; Tong et al., 2012; Castro-Palacio, Nagy, Bemish, & Meuwly, 2014)

A direct way for obtaining an analytical representation of a PES is to use a parametrized functional form(Hutson, 1990; Aguado & Paniagua, 1992) and fit the parameters to a set of *ab initio* data using linear or non-linear least squares procedures.(Law & Hutson, 1997) For the specific case of van der Waals molecules such an approach has been very successful, in particular for applications in spectroscopy.(Hutson, 1990; Roche, Ernesti, Hutson, & Dickinson, 1996) Although such approaches have demonstrated to achieve root mean squared errors (RMSEs) within chemical accuracy,(Boothroyd, Keogh, Martin, & Peterson, 1996) choosing a functional form requires human intuition and the fitting itself can be tedious and

time-intensive.(Meuwly & Hutson, 1999b; Mas et al., 2000)

Over the past years alternative interpolation techniques including the modified Shepard interpolation(Franke & Nielson, 1980; Nguyen, Rossi, & Truhlar, 1995; Bettens & Collins, 1999), the moving least squares method(Lancaster & Salkauskas, 1981; Ischtwan & Collins, 1994; Dawes, Thompson, Wagner, & Minkoff, 2008), permutation invariant polynomials(Cassam-Chenaï & Patras, 2008; Braams & Bowman, 2009; Paukku, Yang, Varga, & Truhlar, 2013) or neural network approaches(Sumpter & Noid, 1992; Bowman et al., 2010; Jiang, Li, & Guo, 2016) have been used to obtain multi-dimensional reactive PESs.(Jordan, Thompson, & Collins, 1995b, 1995a; Skokov, Peterson, & Bowman, 1998; Collins, 2002; Duchovic et al., 2002; X. Zhang, Braams, & Bowman, 2006; J. Li et al., 2012) As an example, the most general expression for a global PES involving 4 atoms using permutation invariant polynomials is(Braams & Bowman, 2009)

$$V(\vec{x}) = \sum_{m=0}^{M} D_{abcdef} \mathcal{S} \left[y_{12}^a y_{13}^b y_{14}^c y_{23}^d y_{24}^e y_{34}^f \right] \tag{4}$$

where the y_{ij}^p are monomials which can, e.g., be Morse-type functions elevated to the power p and the coefficients D_{abcdef} need to be fitted to reference data. The operator $\mathcal{S}[\cdots]$ symmetrizes the monomials. For an A_2B molecule the two possible monomials are $r_{12}^a r_{13}^b r_{23}^c$ and $r_{12}^a r_{23}^b r_{13}^c$ which become $r_{12}^a r_{13}^b r_{23}^c + r_{12}^a r_{23}^b r_{13}^c$ in symmetrized form. The total number of coefficients $D_{a_1 \cdots a_m}$ grows rapidly with the number of atoms. For total polynomial order of 5 and 4 atoms (molecule ABCD with 4 different atoms) there are 462 such coefficients and for 5 atoms (molecule ABCDE) there are 3003 of them. With increasing symmetry (e.g. molecule A_2BCD) the number of distinct polynomials - and hence the number of unique coefficients - decreases. Thus, the number of reference energies that need to be determined depends on the number of distinct coefficients for the fitting problem to be well-defined. Common to all these approaches is the fact that they primarily minimize the RMSE with respect to the training data. In this respect they are similar to parametrized fits which may be acceptable for many cases. As will be discussed next, using reproducing kernel Hilbert space (RKHS) techniques it is possible to reproduce *all* training data *exactly* by construction.

Reproducing Kernel Hilbert Space (RKHS) PES

Machine-learning (ML) methods allow to estimate an unknown function value using a model that was "trained" with a set of known data.(Rupp, 2015) For intermolecular interactions, Rabitz and coworkers(Ho & Rabitz, 1996; Hollebeek, Ho, & Rabitz, 1997, 1999) have popularized the use of reproducing kernel Hilbert space (RKHS) theory,(Aronszajn, 1950) that allows to construct a PES from a training set based on *ab initio* data. Such an approach is typically referred to as kernel ridge regression (KRR) in the ML community.(Hofmann, Schölkopf, & Smola, 2008; Rupp, 2015) The RKHS method has been successfully applied e.g. for constructing PESs for NO+O(Castro-Palacio et al., 2014), N_2^+ + Ar(Unke, Castro-Palacio, Bemish, & Meuwly, 2016) or H_2O.(Ho, Hollebeek, Rabitz, Harding, & Schatz, 1996) A combination of expanding the PES in spherical harmonics for the angular coordinates and reproducing kernels for the radial coordinates has been explored for H_2^+–He(Meuwly & Hutson, 1999b) and is now also used for larger systems.(Dhont, van Lenthe, Groenenboom, & van der Avoird, 2005; van der Avoird, Pedersen, Dhont, Fernandez, & Koch, 2006)

It would be considerably more convenient to supply only a set of *ab initio* data to a toolkit that generates the interpolation (and meaningful extrapolation) of the PES along with all required parameters automatically. One step in this direction has been taken recently by introducing a toolkit for automatically constructing a RKHS of a multidimensional PES from gridded *ab initio* data.(Unke & Meuwly, 2017) A "reproducing kernel Hilbert space" (RKHS) consists of continuous evaluation functionals.(Weinert, 1982) Reproducing kernel Hilbert spaces arise in a number of areas, including approximation theory, statistics, or machine learning.(Hollebeek et al., 1999) In particular, if the values f_i of a function $f(\mathbf{x})$ are known for a set of N training points $\mathbf{x}_i$, it can be shown(Schölkopf, Herbrich, & Smola, 2001) that $f(\mathbf{x})$ can always be approximated as a linear combination of kernel products

$$\widetilde{f}(\mathbf{x}) = \sum_{i=1}^{N} c_i K(\mathbf{x}, \mathbf{x}_i) \tag{5}$$

Here, the c_i are coefficients and $K(\mathbf{x}, \mathbf{x}')$ is the reproducing kernel of the RKHS. The coeffi-

cients c_i satisfy the linear relation

$$f_j = \sum_{i=1}^{N} c_i K_{ij} \tag{6}$$

with $K_{ij} = K(\mathbf{x}_i, \mathbf{x}_j)$ and can therefore be calculated from the known values f_i in the training set by solving

$$\begin{bmatrix} K_{11} & K_{12} & \ldots & K_{1N} \\ K_{21} & K_{22} & \ldots & K_{2N} \\ \vdots & \vdots & \ddots & \vdots \\ K_{N1} & K_{N2} & \ldots & K_{NN} \end{bmatrix} \begin{bmatrix} c_1 \\ c_2 \\ \vdots \\ c_N \end{bmatrix} = \begin{bmatrix} f_1 \\ f_2 \\ \vdots \\ f_N \end{bmatrix} \tag{7}$$

Since the kernel matrix $\mathbf{K} = [K_{ij}]$ is symmetric and positive-definite by construction, Cholesky decomposition(Golub & Van Loan, 2012) can be used to solve Eq. 7. Once the coefficients c_i have been determined, the function value at an arbitrary position $\mathbf{x}$ can be calculated using Eq. 5.

Derivatives of $\widetilde{f}(\mathbf{x})$ of any order can be calculated analytically by replacing the kernel function $K(\mathbf{x}, \mathbf{x}')$ in Eq. 5 with its corresponding derivative. As long as $\widetilde{f}(\mathbf{x})$ approximates $f(\mathbf{x})$ reasonably well, derivatives of $\widetilde{f}(\mathbf{x})$ can be expected to be good approximations of derivatives of $f(\mathbf{x})$.

The explicit form of the multi-dimensional kernel function $K(\mathbf{x}, \mathbf{x}')$ is chosen depending on the problem to be solved. In general, it is possible to construct D-dimensional kernels as tensor products of one-dimensional kernels $k(x, x')$

$$K(\mathbf{x}, \mathbf{x}') = \prod_{d=1}^{D} k^{(d)}(x^{(d)}, x'^{(d)}) \tag{8}$$

where $k^{(d)}$ is the one-dimensional kernel of dimension d and $x^{(d)}$ and $x'^{(d)}$ are the d-th components of the D-vectors $\mathbf{x} = \{x^{(d)}\}$ and $\mathbf{x}' = \{x'^{(d)}\}$, respectively.

If the training set is constructed by scanning through combinations of sets of $N^{(d)}$ points in each dimension, as is usually the case when computing energies from electronic structure methods, the training set is a multi-dimensional grid with a total number N of training

17

points

$$N = \prod_{d=1}^{D} N^{(d)} \tag{9}$$

Here, $N^{(d)}$ can have a different values for each dimension d.

For practical applications in chemical physics it is also of interest to mention that it is possible to handle incomplete grids with an RKHS interpolation.(Hollebeek et al., 1999) This is important because even for triatomic systems it may happen that converging quantum chemical calculations turns out to be difficult for certain geometries. Under these circumstances the grid of target energies contains a "hole".

In order to put RKHS into practical use, kernel functions $k(x, x')$ have to be chosen. One particular advantage is that physical knowledge (e.g. appropriate asymptotic - long range - decay) can be encoded in a radial kernel function. This sets them apart from permutationally invariant polynomials(Cassam-Chenaï & Patras, 2008; Bowman et al., 2010), Gaussian approximated potentials (GAP)(Bartok & Csanyi, 2015), or PES constructed from Gaussian processes.(Kolb, Marshall, Zhao, Jiang, & Guo, 2017) Permutational invariance for RKHS interpolations can be achieved because any symmetry in the data is preserved by the symmetry of the kernels.

Explicit radial kernels include the reciprocal power decay kernel

$$k_{n,m}(x, x') = n^2 x_>^{-(m+1)} B(m+1, n) {}_2F_1\left(-n+1, m+1; n+m+1; \frac{x_<}{x_>}\right) \tag{10}$$

or the exponential decay kernel

$$k_n(x, x') = \frac{n \cdot n!}{\beta^{2n-1}} e^{-\beta x_>} \sum_{k=0}^{n-1} \frac{(2n-2-k)!}{(n-1-k)!k!} [\beta(x_> - x_<)]^k \tag{11}$$

where $x_>$ and $x_<$ are the larger and smaller of x and x' and the integer n determines the smoothness. In Eq. 10 the parameter m is the long-range decay of the dominant intermolecular interaction (e.g. $m = 6$ for dispersion), $B(a, b)$ is the beta function and ${}_2F_1(a, b; c; d)$ is the Gauss hypergeometric function.

Recently, RKHS-interpolated PES have not only been used for spectroscopy(Meuwly & Hutson, 1999b) but also for reactive (bond-breaking/bond-formation) processes ranging from triatomics to ligand binding in proteins.(Castro-Palacio et al., 2014; Soloviov & Meuwly, 2014, 2015) For low-dimensional systems it is now possible to obtain RKHS representations(Unke & Meuwly, 2017) for thousands of reference *ab initio* calculations which can be used in running statistically significant numbers of QCT trajectories(Castro-Palacio et al., 2014; Unke et al., 2016; Yosa Reyes et al., 2016; Brickel & Meuwly, 2017) or to solve the nuclear Schrödinger equation.(Denis-Alpizar, Unke, Bemish, & Meuwly, 2017) In fact, the toolkit was applied to the interpolation of a six-dimensional function based on more than 7×10^6 points.(Unke & Meuwly, 2017) For high-dimensional problems the total energy is decomposed into a part described by a RKHS PES and an environmental part describe by an empirical force field(Soloviov & Meuwly, 2014, 2015) akin to mixed quantum mechanical (QM)/molecular mechanics (MM) simulations.

In summary, representing gridded data from electronic structure calculations using RKHS approaches has the advantage that the interpolant *exactly* reproduces the reference energies and has guaranteed (and smooth) behaviour at long and short distances as built-in features in the kernel function.

Existing Implementations

An EVB implementation is available within the MOLARIS package.(Warshel et al., 2012) More recently, EVB has also been made available in CHARMM(Glowacki et al., 2015), TINKER(Carpenter, Harvey, & Glowacki, 2015) and Q6.(Bauer et al., n.d.). Temporal MS-ARMD(Nutt & Meuwly, 2006; Danielsson & Meuwly, 2008) and MS-ARMD based on energy mixing(Nagy et al., 2014) have been implemented in CHARMM. Molecular mechanics with proton transfer(Lammers et al., 2008) and MS-ARMD with VALBOND(Tubert-Brohman et al., 2009; Schmid et al., 2018) (for metal force fields) are also available within CHARMM. In all these cases the essential step is fitting the force fields together with the features connecting them (off-diagonal elements or GAPOs, respectively) which is, as yet, not automated.

Applications

Dynamics studies of chemical reactions date back more than 50 years.(Karplus et al., 1964) Since then the sophistication of the PESs and the accuracy with which the nuclear dynamics can be followed have continuously increased.(Bowman, Czako, & Fu, 2011) In the following a number of recent attempts primarily aimed at quantitative studies of chemical reactions in the gas- and condensed-phase are summarized.

Small Molecule Reactions

Reaction Dynamics in the Hypersonic Regime: Particularly interesting applications of reactive MD simulation concern physical conditions that are difficult to achieve in laboratory experiments, such as extremely high ($T \geq 10000$ K) temperatures as they occur in explosions or in hypersonics.(Millikan & White, 1963) The O(^{3}P) + NO($^2\Pi$) $\rightarrow$ O$_2$($X^3\Sigma_g^-$) + N(^{4}S) reaction(Gilibert, Aguilar, Gonzalez, & Sayos, 1993; Gilibert, Gimenez, Gonzalez, Sayos, & Aguilar, 1995; Bose & Candler, 1997; Balakrishnan & Dalgarno, 1999; Defazio, Petrongolo, Gray, & Oliva, 2001; Defazio, Petrongolo, Oliva, Gonzalez, & Sayos, 2002; Gonzalez, Oliva, & Sayos, 2002; Caridade & Varandas, 2004; J.-J. Ma, Chen, Cong, & Han, 2006; Castro-Palacio et al., 2014; Castro-Palacio, Bemish, & Meuwly, 2015) is one such example which plays an important role for the energetics of the reactive air flow around spacecraft during hypersonic atmospheric reentry. This process is also known as the Zeldovich reaction which produces active nitrogen from molecular nitrogen (N$_2$) in the gas phase(Zeldovich, 1946) which becomes important above $\sim$ 2000 K.
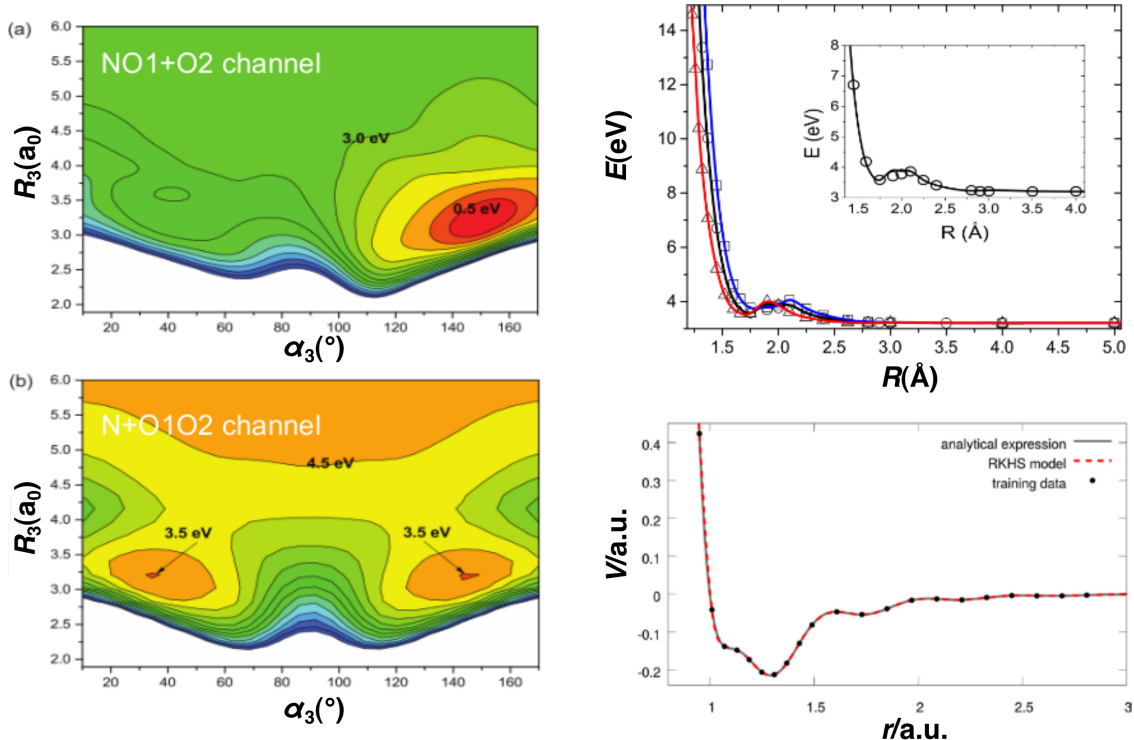
Figure 3: Contour plots for the NO1+O2 (panel a) and O2O1+N (panel b) grids in R_1, α_1 and R_3, α_3 Jacobi coordinates, respectively. The N-O1 (r_1) and O2-O1 (r_3) distances are 2.25 a_0 and the contour levels are separated by 0.5 eV. Panel c: MRCI+Q/cc-pVQZ energies along the R coordinate for $r = 1.21A$ (N-O1 distance) and $\alpha = 27.5, 34.0$ and $43.1°$ (squares, circles and triangles, respectively). The solid lines are RKHS interpolants. The inset in the graph represents a close-up of the cut for $\alpha = 34.0°$ which is not used for the RKHS interpolation. Panel d: Performance of the RKHS method for the function $V(r) = \left(\frac{1}{r^9} - \frac{1}{r^6}\right)\left(\cos^2(7r) + 1\right)$. The RKHS interpolant $\widetilde{f}(\mathbf{x})$ (red dashed line) constructed from the training samples (black dots) is virtually identical to the analytical expression (grey line). Panels a to c and d adapted from Refs.(Castro-Palacio et al., 2014; Unke & Meuwly, 2017).

The potential energy surfaces for this reaction range from Sorbie-Murrell potentials using contracted configuration interaction (CCI) calculations(Gilibert et al., 1993; Bose & Candler, 1997) to an RKHS-interpolated PES (see Figure 3) based on MRCI+Q calculation with large basis sets.(Castro-Palacio et al., 2014) The Sorbie-Murrell potential is based on a diatomics-

in-molecule expansion combined with a many body expansion.(Sorbie & Murrell, 1975; Gilibert et al., 1993) Further along these lines, a DIM-based double many body expansion (DMBE) PES has been developed(Varandas, 2003) and used in QCT simulations.(Caridade & Varandas, 2004) Using this DMBE PES the rate $k_+(T)$ for the forward reaction (N+O$_2$ → NO+N) was determined from QCT simulations and that for the reverse reaction ($k_-(T)$ from statistical mechanics. Combining the two, the equilibrium rate $K(T) = \frac{k_+(T)}{k_-(T)}$ was found to be in good agreement with reference data.(Chase et al., 1985) A shortcoming of this approach is that the forward and reverse rate coefficients were determined using different methods which was done because the low reaction probability requires extensive sampling.
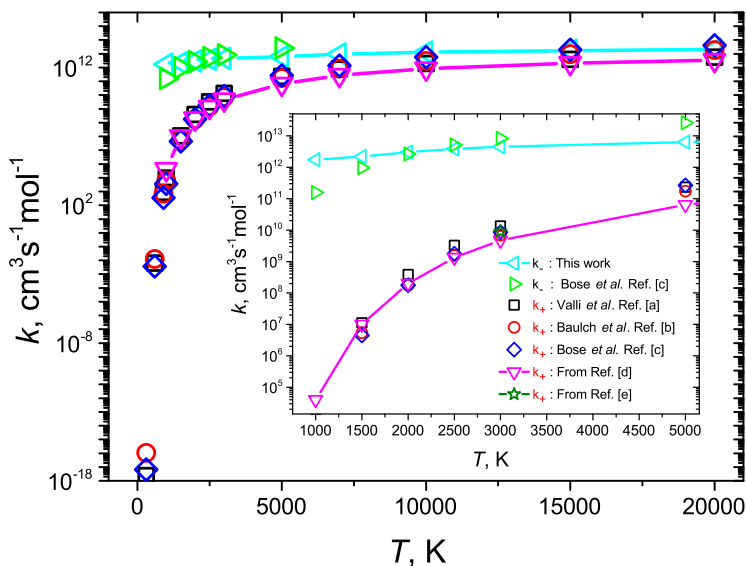
Figure 4: Rate coefficients $k_-(T)$ (blue open triangles) and $k_+(T)$ (red open triangles) for the NO($X^2\Pi$)+N(^4S) ↔ N$_2$($X^1\Sigma$)+O(^3P) reaction for $300 \leq T \leq 20000$ K. The inset shows results for $1000 \leq T \leq 5000$ K. The labels correspond to references: [a]=Ref.(Valli et al., 1995), [b]=Ref.(Baulch et al., 1994), [c]=Ref.(Bose & Candler, 1997), [d]=Ref.(Castro-Palacio et al., 2014), and [e]=Ref.(T. Clark et al., 1969). Figure adapted from Ref.(Castro-Palacio et al., 2015)

Using the fully reactive RKHS-PES, $k_+(T)$ and $k_-(T)$ were determined from explicit QCT simulations(Castro-Palacio et al., 2015) and compared with experimental data. A comparison of the forward and reverse rates is provided in Figure 4. For $k_+(T)$ it is found that an experimentally measured data point at 3000 K (green star) agrees very favorably with the atomistic simulations (magenta) which provide a benchmark for the computations. Comparison of the equilibrium rate $K(T)$ with those from the CEA database (Gordon & McBride, 1996; McBride, Zehe, & Gordon, 2002) shows very favourable agreement for temperatures $T > 5000$ K.

For the related $NO(X^2\Pi)+N(^4S) \leftrightarrow N_2(X^1\Sigma)+O(^3P)$ reaction fully-dimensional, global potential energy surfaces have also been computed.(Gamallo, Gonzalez, & Sayos, 2003; Lin, Varga, Song, Paukku, & Truhlar, 2016; Denis-Alpizar, Bemish, & Meuwly, 2017) Based on CASPT2 calculations a many-body expansion was fitted and used for variational transition state calculations(Gamallo et al., 2003) and QCT simulations.(Esposito & Armenise, 2017) A more recent effort used a least-squares fit of permutationally invariant polynomials to dynamically scaled MRCI energies.(Lin, Varga, et al., 2016) These PESs have then been used in subsequent QCT simulations.(Lin, Meana-Paneda, Varga, & Truhlar, 2016) This work focused on the scattering process and found that the fraction of NO deflected in the forward direction decreases with increasing collision energy. Complementary to this, RKHS-interpolated PESs based on MRCI+Q calculations were used to determine rate coefficients for different reaction channels for temperatures up to 20000 K, see Figure 4.(Denis-Alpizar, Bemish, & Meuwly, 2017) From the QCT simulations the rates $k(T)$ for $5000 \leq T \leq 20000$ can be fit to an Arrhenius expression

$$k^{\text{exch}}(T) = 1.475 \times 10^{-10} \exp(-20907.67/T) \tag{12}$$

and

$$k^{\text{form}}(T) = 1.712 \times 10^{-10} \exp(-7423.430/T) \tag{13}$$

for the exchange and N_2 formation processes, respectively.

The QCT simulations and quantum wavepacket simulations reveal the non-equilibrium char-
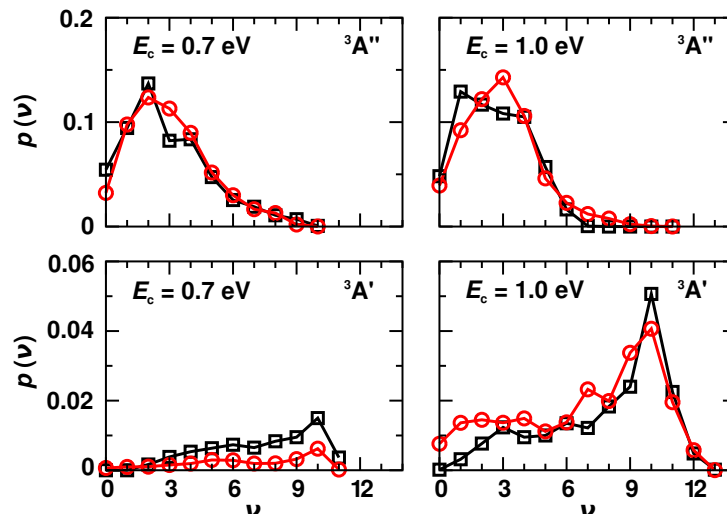
Figure 5: Vibrational energy distribution $p(\nu)$ for the N_2 product following the $NO(\nu = j = 0)+N \rightarrow N_2+O$ reaction with $J = 0$ from time independent (red lines with circles) and QCT (black line with squares) simulations on both PESs, $^3A'$ and $^3A''$. Figure adapted from Ref.(Denis-Alpizar, Bemish, & Meuwly, 2017).

acter of the N_2−product state distributions for the vibrational degree of freedom for collisional processes at high temperature. It is also found that quantum effects at such high temperatures are moderate (see Figure 5) and lead to differences in the percent range for product state distributions. Microscopic information about $k(T)$ and $p(\nu)$ is essential for the macroscopic modeling of the reactive flow around objects in the hypersonic flight regime.(Martin & Boyd, 2011) More generally, the results on N+NO and O+NO reactive scattering based on RKHS-interpolated PESs from high-level (MRCI+Q or similar) electronic structure calculations together with QCT or quantum dynamics simulations suggest that this is a generic framework to obtain reliable microscopic information under conditions that are difficult or even impossible to probe in a controlled laboratory environment.

Vibrationally induced reactivity: Reactions following the excitation of vibrational overtones are potentially relevant in atmospheric chemistry. Experimentally, such processes are challenging to study because preparing molecules in the gas phase with sufficient energy in one of the vibrations is difficult due to the small excitation cross sections for higher excited

states.(Crim, 1993) Hence, computations provide a meaningful complement to such studies.

A particularly topical example is the decomposition of HSO_3X (X = OH, F, Cl) which is of considerable relevance in atmospheric chemistry(Rosen & Hofmann, 1983; Burkholder, Mills, & McKeen, 2000; Hintze, Kjaergaard, Vaida, & Burkholder, 2003; Vaida et al., 2003). It had been assumed that photodissociation of H_2SO_4 would proceed via ultraviolet (UV) radiation. However, the electronic absorption spectrum of H_2SO_4 above 140 nm could not be found(Burkholder et al., 2000; Hintze et al., 2003; Vaida et al., 2003; Wrenn, Butler, Rowland, Knox, & Phillips, 1999; Robinson, Schofield, & Kjaergaard, 2003) and UV photons with wavelengths shorter than 179 nm are efficiently absorbed at higher altitudes which makes UV photodissociation unlikely to occur at lower altitudes.(Burkholder et al., 2000) This lead to the proposal that vibrational overtone excitation of the OH stretch mode could drive photodissociation of H_2SO_4.(Donaldson, Frost, Rosenlof, & Tuck, 1997; Vaida & Donaldson, 2014)

In a first computational study, the photodissociation dynamics following excitation with $\nu_9 = 4$ to 6 quanta in the OH-stretching vibration was investigated by semiempirical (PM3) classical trajectory simulations.(Y. Miller & Gerber, 2006) This was followed by extensive MS-ARMD simulations using separate force field parametrizations for the reactant (H_2SO_4) and product ($SO_3 + H_sO$) states.(Yosa Reyes et al., 2014) The quality of this parametrization, based on MP2/6-311G++(2d,2p) calculations, is reported in Figure 6. From several 1000 independent trajectories with excitations of $\nu_9 = 4$ to 6 quanta the probability distribution for the reaction time for photodissociation were determined. With increasing excitation of the OH stretch the average reaction times decrease from 19.5 ns for $\nu_9 = 4$ to 31 ps for $\nu_9 = 6$.(Yosa Reyes et al., 2014) Here it is important to note that water elimination from this nonequilibrium ensemble is characterized by a *distribution* of reaction times $p(\tau)$ which can only be characterized if a statistically significant number of MD trajectories is run.(Yosa & Meuwly, 2011) For this system, 1 ns of *ab initio* MD simulations at the MP2/6-311G++(2d,2p) level of theory would be extremely challenging ($\sim$ years), depending on the hardware available which is clearly impractical.
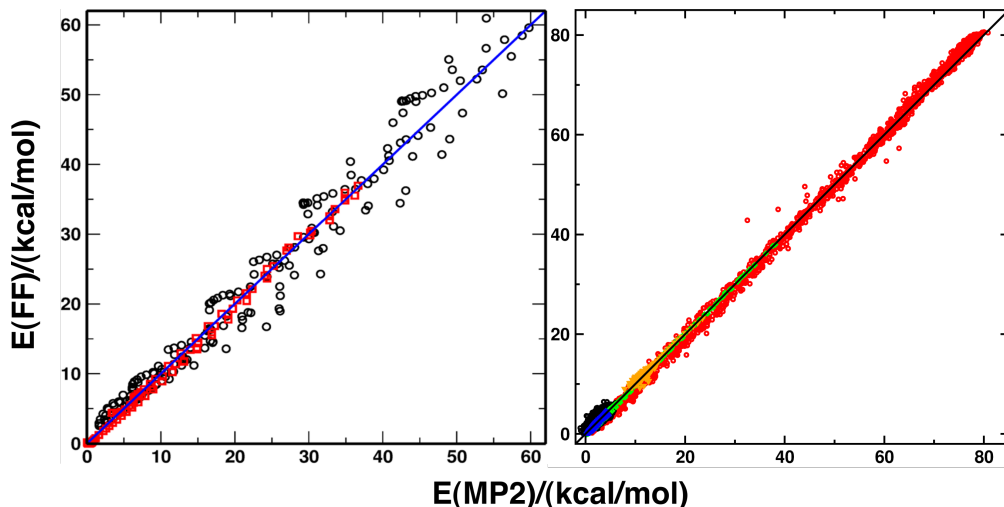
Figure 6: Quality of the reactive force fields for the photodissociation of H_2SO_4 (left) and HSO_3F (right). In the left panel, points along the minimum energy paths are red squares and the remaining training points from finite-temperature MD simulations are black circles. In the right panel, the red, black, green, blue and yellow symbols correspond to sampling the $\nu_{OH} = 6$ overtone, HSO_3Cl at 300 K, the minimum energy path, the dihedral dynamics, and the $HCl+SO_3$ complex, respectively. Adapted from Refs.(Yosa Reyes et al., 2014, 2016)

Condensed-Phase Reactions

Originally, (MS-)ARMD has been developed for ligand rebinding reactions in proteins, such as NO- rebinding to Myoglobin (Mb)(Nutt & Meuwly, 2006; Danielsson & Meuwly, 2008) or Histidine binding and unbinding in neuroglobin(Nienhaus, Lutz, Meuwly, & Nienhaus, 2013) using empirical force fields. The purpose was to directly follow the dynamics across the (high-dimensional) transition seam and to avoid treating the ligand-bound and ligand-unbound states separately.(Meuwly et al., 2002) Such a protocol also allows recrossing to take place which is one of the more serious deficiencies of transition state theory. Following the introduction of MS-ARMD(Nagy et al., 2014), the protocol was also combined with RKHS-interpolated PESs for the most important degrees of freedom involved in the reaction.(Soloviov & Meuwly, 2014, 2015) This not only provided the functionality of bond-

breaking and bond-formation but also the necessary accuracy to make direct contact with experiment.(Soloviov, Das, & Meuwly, 2016) Used in this fashion, MS-ARMD with RKHS is akin to a mixed quantum mechanical (QM)/molecular mechanics (MM) approach which treats part of the system with a "high accuracy" method (QM) whereas the remaining degrees of freedom are represented as an empirical force field (MM)(van der Kamp & Mulholland, 2013) The advantage, however, is that the energies and forces in MS-ARMD are evaluated at MM-speed and a statistically significant number of explicit MD simulations can be run due to the dramatically increased speed.

Nitric Oxide Rebinding in Myoglobin: A topical application of MS-ARMD/RKHS-simulations is the rebinding of nitric oxide to myoglobin. Nitric oxide is a physiologically relevant ligand(Pacher, Beckman, & Liaudet, 2007; Lundberg et al., 2009; Traylor & Sharma, 1992) which binds reversibly to the heme-active site of Mb. Experimentally, the rebinding kinetics of NO to the heme-group involving the bound ^2A and unbound ^4A states has been studied extensively, including UV/visible(Cornelius, Hochstrasser, & Steele, 1983; Petrich et al., 1991; Ionascu et al., 2005), mid-IR(Kruglik et al., 2010; J. Kim et al., 2012; Yoo et al., 2012; S. Kim, Jin, & Lim, 2004) and resonance Raman(Kruglik et al., 2010) techniques. In all cases the rebinding kinetics is multi-exponential with time constants on the 10 ps time scale and those on the 100 ps time scale.(Petrich et al., 1991; Kruglik et al., 2010; J. Kim et al., 2012; Yoo et al., 2012; Nutt & Meuwly, 2006; Danielsson & Meuwly, 2008)

One of the important protein degrees of freedom in this process is the Fe-out of plane (Fe-oop) motion. Upon ligand dissociation, which changes the iron coordination from octahedral to pyramidal, the iron moves below the plane towards the proximal histidine, His93 in WT Mb. Using a 3-dimensional RKHS-based PES $V(R, \theta, \phi)$ for the ligand (R and θ) and Fe-oop (ϕ) degrees of freedom, the ^{2}A and ^{4}A PESs are represented as

$$V(R, \theta, \phi) = \sum_{\lambda=0}^{10} V_\lambda(R, \phi) P_\lambda(\cos(\theta)) + V_{\mathrm{lr}}(\phi) \tag{14}$$

where P_λ are Legendre polynomials, V_λ are radial strength functions, and V_{lr} describes the doming in the asymptotic, long range region $R \to \infty$ and is represented as a harmonic

potential:

$$V_{\mathrm{lr}}(\phi) = \frac{1}{2}k(\phi - \phi_e)^2 \tag{15}$$

k is the force constant and ϕ_e is the equilibrium position. The radial strength functions $V_\lambda(R, \phi)$ are represented as a reproducing kernel

$$V_\lambda(R, \phi) = \sum_{i,j} \alpha_{\lambda,i,j} \cdot \mathcal{K}(R, R_i) \cdot \mathcal{G}(\phi, \phi_j) \tag{16}$$

where $\mathcal{K}(R, R_i)$ is a radial kernel(Ho & Rabitz, 1996; Hollebeek et al., 1999) and $\mathcal{G}(\phi, \phi_j)$ is a Gaussian kernel.(Hangelbroek & Ron, 2010) The $\alpha_{\lambda,i,j}$ are coefficients which follow from a singular value decomposition.(Hestenes, 1958; Golub & Kahan, 1965) In parametrized form, the radial reproducing kernels are

$$\mathcal{K}(R, R_i) = \frac{1}{14}r_>^{-7}\left(1 - \frac{7}{9}\frac{R_<}{R_>}\right) \tag{17}$$

where $R_>$ and $R_<$ are the greater and smaller distance, respectively, for any pair of $R-$values. The Gaussian kernel is defined as

$$\mathcal{G}(\phi, \phi_j) = \exp\left(-\frac{(\phi - \phi_j)^2}{2\sigma}\right) \tag{18}$$

where σ is the width of the kernel.

The force field for the bound and unbound state was validated(Soloviov & Meuwly, 2015) vis-a-vis experimental data from optical spectroscopy.(Lim et al., 1993) After breaking the Fe-NO bond the Fe immediately starts to move below the heme-plane on a ~ 100 fs time scale and the relaxation dynamics extends over several 10 ps. Using the RKHS PES for the unligated state the decay follows a double exponential $ae^{-t/\tau_1} + be^{-t/\tau_2}$ with $\tau_1 = 3.5$ ps and $\tau_2 = 64.4$ ps, as shown in Figure 7. This compares with time constants of $\tau_1 = 3.5$ ps and $\tau_2 = 83.0$ ps from the experiments.(Lim et al., 1993) Starting from a thermal ensemble of the ligated MbNO state, a statistically significant number of MS-ARMD rebinding trajectories for the fully hydrated system was run. Each trajectory for which the photodissociated ligand rebinds provides an individual rebinding time from which the fraction of rebound systems, $N(t)$, can be determined. The rebinding kinetics on the sub-nanosecond time scale follows a multiexponential decay with two time constants $\tau_1 \approx 10$ ps and $\tau_2 \approx 150$ ps, depending on the
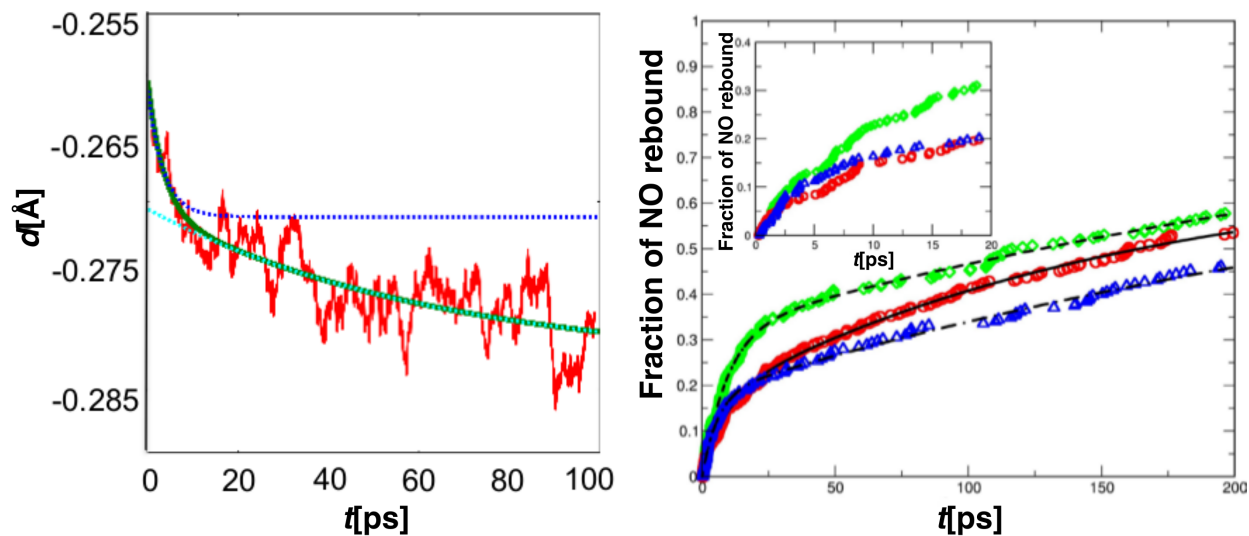
Figure 7: Left: Time dependence of the Fe-oop motion after photodissociation of the ligand and subsequent dynamics on the ^4A PES. The black line is the fit to $d(t) = ae^{-t/\tau_1} + be^{-t/\tau_2}$ and the blue and green lines are the experimentally determined exponential decays.(Lim et al., 1993) Right: NO-rebinding kinetics depending on the value of the asymptotic separation Δ. Adapted from Refs.(Soloviov & Meuwly, 2015; Soloviov et al., 2016)

asymptotic separation Δ of the two states which is a conformationally averaged quantity that relates the total energies of the two MS-ARMD/RKHS force fields.(Danielsson & Meuwly, 2008) The value for Δ can be approximately calculated from electronic structure calculations but will eventually have to be fitted to reproduce experimental observables.(Danielsson & Meuwly, 2008) For a value of $\Delta = -6.12$ kcal/mol the rebinding efficiency within 200 ps is ~ 55 % which compares with a value of 75 % from recent XAS measurements on the same time scale.(Soloviov et al., 2016; Silatani et al., 2015) Decreasing the value to $\Delta = -3.12$ kcal/mol yields quantitative agreement for the rebinding times and the rebound fraction.

Additional information about structural changes accompanying the ligand binding and un-binding process has been obtained from X-Ray absorption (XAS) experiments.(Silatani et al., 2015) For an ensemble of structures from equilibrium simulations in the bound and unbound states the conformationally averaged XANES spectra and their difference spectrum has been determined. The computed difference spectrum almost quantitatively agrees with the ex-

perimentally measured transient after 50 ps. It had been suggested that such experiments are sensitive to the photodissociated ligand being "close to" or "far away" from the heme-Fe in the active site.(Silatani et al., 2015) However, the simulations demonstrate that such details can not be quantified from the experiments within the signal-to-noise of the experiment.

The real value of such validated MS-ARMD/RKHS-MD simulations is the fact that all structural and dynamical information is available from the aggregate simulations and can be analyzed in view of very specific questions. One of the unresolved points in NO-rebinding to myoglobin was the structural interpretation of the two observed rebinding times on the 10 ps and 100 ps time scale, respectively. Because the transition state of a chemical reaction is metastable with very short lifetime it can usually not be characterized directly using experiments. In the simulations it is, however, possible to cluster trajectories that rebind on particular time scales and investigate common and distinguishing features between them. This was done for NO rebinding to Mb by separately analyzing the ensemble of trajectories that rebind on the 10 ps and 100 ps time scale.(Soloviov et al., 2016) Such an analysis demonstrates that on the short time scale the His64 residue occupies a region away from the heme-iron which leaves the Fe-atom available for NO-rebinding. Contrary to that, for longer rebinding times (100 ps) the entire histidine side chain pushes towards the heme-iron and occludes it. For NO-rebinding to take place the His64 side chain needs to move away from this position. The two discrete states available to the His64 side chain are separated by a free energy barrier of ≈ 2 kcal/mol which is consistent with interconversion times of a few hundred picoseconds, observed previously.(Merchant et al., 2003; J. Ma, Huo, & Straub, 1997)

The combination of validated MS-ARMD/RKHS force fields for the ^2A and ^4A states of MbNO with statistically significant sampling of the rebinding dynamics provides a molecularly refined picture of the reactive process and a structural interpretation of the two experimentally known time scales.(Petrich et al., 1991) Directly linking rebinding time scales and structural dynamics from experiment alone appears extremely difficult and quantitative atomistic simulations provide the missing link for this.

Competitive Ligand Binding in Truncated Hemoglobin N: MS-ARMD with conventional force fields was recently also applied to the competitive rebinding of NO and O_2 in the active site of truncated Hemoglobin N (trHbN).(Das & Meuwly, 2018) The dioxygenation reaction converts harmful nitric oxide to benign nitrate in bacteria(Poole & Hughes, 2000) and is relevant for NO-detoxification in blood.(Bang et al., 2006; Tinajero-Trejo et al., 2014; Kollau et al., 2016; Carabet, Guertin, Lague, & Lamoureux, 2017) The reaction was first studied for Myoglobin (Mb)(Doyle & Hoekstra, 1981) followed by studies focusing on nitrate formation in other globins using experimental and computational approaches(Eich et al., 1996; Herold, Exner, & Nauser, 2001; Gladwin, Lancaster, Freeman, & Schechter, 2003; Mishra & Meuwly, 2010). From stopped flow experiments, the second order rate constants for the reaction of NO with oxyHb and oxyMb (process III, see equation 19) are 4.36×10^7 and 8.9×10^7 M^{-1} s^{-1}, respectively(Eich et al., 1996; Herold et al., 2001; Gladwin et al., 2003).

$$
\begin{array}{ccccc}
 & & \text{I} & & \\
\mathrm{Fe^{II}-NO} + O_2 & \longrightarrow & \mathrm{Fe^{II}-O_2} + \mathrm{NO} & \longrightarrow & \mathrm{Fe^{III}} + \mathrm{NO_3^-} \\
 & \text{II} & & \text{III} &
\end{array}
\tag{19}
$$
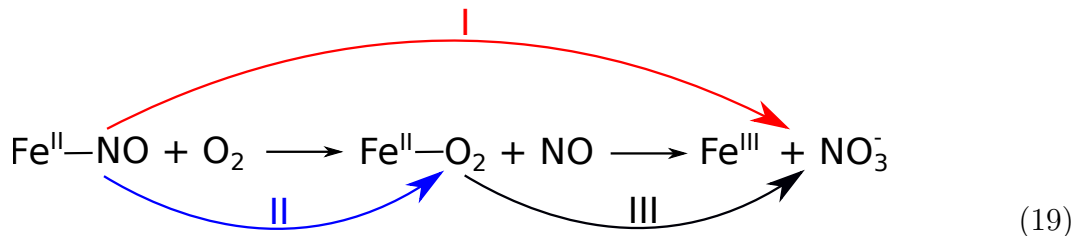
Because electronic structure calculations for Fe-O_2 complexes are notoriously difficult(Jensen & Ryde, 2004; Franzen, 2002; Kepp, 2013; Siegbahn, Blomberg, & Chen, 2010; Ali, Sanyal, & Oppeneer, 2012) the Fe-NO and Fe-O_2 interactions were parametrized solely on experimental data.(Das & Meuwly, 2018) Based on such a parametrization of the system MS-ARMD and umbrella sampling simulations for the free energy of ligand exchange were carried out. The free energy barrier associated with the $\mathrm{Fe^{II} - NO} + O_2 \rightarrow \mathrm{Fe^{II} - O_2} + \mathrm{NO}$ reaction is 19.7 kcal/mol, see Figure 8. Using transition state theory, such a barrier corresponds to a rate of 4.5×10^{-3} s^{-1} which agrees well with rates from experiments (Process I, see equation 19) ranging from 1.0×10^{-4} to 4.4×10^{-3} s^{-1} depending on the protein considered and confirms that the ligand exchange reaction (process II, see equation 19) is the rate limiting step(Ascenzi, Bolognesi, & Visca, 2007; Ascenzi, Gullotta, Gioia, Coletta, & Fasano, 2011).

This is also consistent with the fact that process III (Fe-O$_2$ + NO $\rightarrow$ Fe(III) + NO$_3^-$) is fast as it occurs on the 10 to 100 ps time scale(Mishra & Meuwly, 2010).
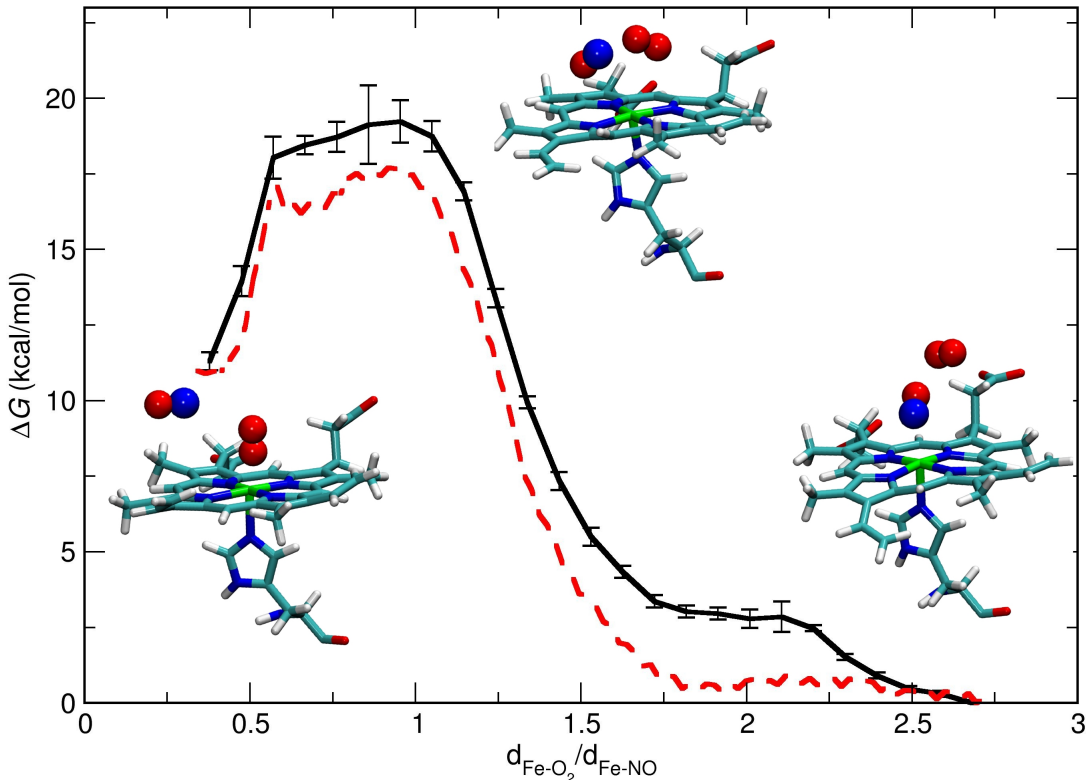
Figure 8: Free energy profile including error bars for the ligand exchange reaction in WT trHbN from umbrella sampling (black trace) along the reaction coordinate $\rho = \frac{d_{\text{Fe}-\text{O2}}}{d_{\text{Fe}-\text{NO}}}$. The structures of O$_2$-bound ($\rho = 0.25$), NO-bound ($\rho = 2.5$) and the transition state ($\rho \sim 1.0$) are also shown. The TS region is broad and involves a distributed structural ensemble. The red dashed line shows the free energy profile for the ligand exchange reaction for the Y33A mutant. Adapted from Ref.(Das & Meuwly, 2018)

Analysis of the structural dynamics of the Gln58 residue between the reactant and the TS suggests that this residue does not participate appreciably in the reaction and hence the overall rate should depend little on mutating this residue. Indeed, experiments find only an insignificant rate increase from $(2.2 \pm 0.3) \times 10^8$ M^{-1}s^{-1} (WT) to $(2.6 \pm 0.4) \times 10^8$ M^{-1}s^{-1} (Q58A) for nitrate formation.(Koebke, Waletzko, & Pacheco, 2016) Conversely, probability distribution functions for Tyr33 and Val80 differ appreciably between reactant and TS. Con-

comitantly, the rate coefficients increase by more than a factor of two (and hence the free energy barrier decreases by ≈ 1.7 kcal/mol based on transition state theory) upon Alanine mutation of these two residues, to $(4.6 \pm 0.9) \times 10^8$ M^{-1}s^{-1} and $(4.7 \pm 0.6) \times 10^8$ M^{-1}s^{-1}, for the Y33A and V80A mutants, respectively.(Koebke et al., 2016).

Umbrella sampling of the free energy surface and reaction barrier height for ligand exchange in the Y33A mutant find that the barrier height for the $Fe^{II} - NO + O_2 \rightarrow Fe^{II} - O_2 + NO$ reaction is lowered by $\Delta\Delta G = 1.5$ kcal/mol compared to WT. This result is in quantitative agreement with the value determined from experiment (~ 1.7 kcal/mol). Hence, the difference between WT and the Y33A mutant can be traced back to the stabilizing interaction between the ligands and the -OH group of the Tyrosine at position 33 in the WT protein which is absent in the Alanine-mutant.

Analysis of the pocket volumes in the TS indicates an expansion by more than 10 % in pocket volume between the WT (197 Å^3) and Y33A mutant (234 Å^3). This increases entropy and hence reduces the free energy and the barrier for rebinding. The decreased barrier for Y33A may be due to favorable entropic contributions. An enthalpic origin of that magnitude is unlikely due to the small dipole moments of both ligands. This was explicitly verified by computing average interaction energies (over 500 structures from 1 ns simulation in the TS) between the ligand and the surrounding protein which are -3.83 kcal/mol for the WT compared with -3.40 kcal/mol for the Y33A mutant i.e only a difference of $\Delta H = 0.4$ kcal/mol compared to $\Delta G = 1.5$ kcal/mol, leaving $-T\Delta S = 1.1$ kcal/mol for the entropic contribution of the overall process. It is also of interest to note that the interaction energies of the free ligands in the WT reactant (Fe-NO) and product (Fe-O$_2$) states are –2.7 and –2.8 kcal/mol, respectively, which suggests that in moving to the transition state a certain amount of entropic penalty is to be paid due to spatial constraints.

OUTLOOK

Reactive force fields provide molecularly refined interpretations of chemical reactions in the gas and condensed phase. This concerns both, thermodynamic and kinetic aspects of chemical transformations. Despite the successes, the representation and fitting of such FFs is still a laborious process. For routine and broader application in the area of atomistic simulations, improved fitting strategies are required. In the following, a few novel developments based on machine learning (ML) are outlined.

In 1929 Paul Dirac(Dirac, 1929) noted that the (electronic and nuclear) Schrödinger equation (SE) contains all that is necessary to describe chemical phenomena and processes. As the underlying equation (SE) is too complicated to be solved in closed form but for the simplest systems, computational and numerical methods have been devised to find approximate solutions such that meaningful information about a system and/or a process can be obtained. Instead of approximating solutions either by resorting to "mean-field" or "perturbative" solutions within a Density functional Theory (DFT) or *ab initio* electronic structure framework or entirely empirical, parametrized energy functions it may also be possible to exploit the fact that the electronic Hamiltonian $\hat{H}$ is uniquely determined by the external potential, which in turn depends only on the set of nuclear charges $\{Z_i\}$ and atomic positions $\{\mathbf{r}_i\}$ of the system. Providing a sufficiently large number of precomputed data (typically energies) to estimate properties for unknown compounds or structures(Rupp, Tkatchenko, Müller, & Von Lilienfeld, 2012; Montavon et al., 2013; Hansen et al., 2013, 2015) it has become possible to avoid to explicitly but only approximately solving the electronic Schrödinger equation. Instead, a computer system learns to predict energies based on an increasing amount of data.

Artificial neural networks (NNs)(McCulloch & Pitts, 1943; Kohonen, 1988; Abdi, 1994; Bishop, 1995; J. W. Clark, 1999; Ripley, 2007; Haykin, 2009) are a popular class of ML algorithms to tackle computationally demanding problems.(Hinton et al., 2012; Lawrence, Giles, Tsoi, & Back, 1997). Specifically, NNs have been used previously to fit PESs for molecular systems in the spirit of many-body expansions(Manzhos & Carrington Jr, 2006,

2007; Malshe et al., 2009; Handley & Popelier, 2010). While being accurate, they typically involve a large number of individual NNs (one for each term in the many-body expansion), making the method scale poorly for large systems. An alternative approach, known as high-dimensional NN (HDNN) first applied to bulk silicon,(Behler & Parrinello, 2007; Behler, 2011) decomposes the total energy of a system into atomic contributions, which is appealing, because "energy" is an extensive property and it allows to apply the same network to systems of different size.

A conceptually different approach, the deep tensor NN (DTNN)(Schütt, Arbabzadah, Chmiela, Müller, & Tkatchenko, 2017), allows to reuse the same NN to predict energies of systems with different composition across chemical space. Similar to HDNNs, DTNN accumulates atomic energy contributions to predict the total energy E_{tot}.More recently, the SchNet architecture was proposed(Schütt, Kindermans, et al., 2017), which improves upon the DTNN. When trained on 100k reference structures, SchNet predicts the energy of structures in the QM9 dataset(Ramakrishnan, Dral, Rupp, & Von Lilienfeld, 2014) with a mean average error (MAE) of 0.34 kcal mol^{-1}.

Using a strictly local chemical descriptor, a NN-based method tailored for accurate energy evaluations, which can be applied to construct PESs for nonreactive and reactive dynamics of chemically heterogeneous systems in the condensed phase, has been introduced.(Unke & Meuwly, 2018) Such a NN trained on 100k reference structures can learn to accurately predict energies of structures in the QM9 dataset(Ramakrishnan et al., 2014) across chemical space with a MAE of 0.41 kcal/mol which is only slightly worse than that of the SchNet architecture(Schütt, Kindermans, et al., 2017) (MAE of 0.34 kcal/mol). Contrary to SchNet, this NN is considerably more efficient because a local descriptor is used and the network architecture is much simpler. In addition, the approach was also applied to 100k reference structures from a reactive MD simulation of malonaldehyde. It was found that they can be reproduced with mean average errors between 0.1 and 0.4 kcal/mol. As forces can also be evaluated it will be possible to train NN for reactive MD simulations. However, it should be remembered that developing NN-based energy functions depends on the availability of

massive amounts of training data (typically 10^5 or more reference energies are required).

Similar to a combination of RKHS-based and empirical FFs together with MS-ARMD to combine accurate representations of intermolecular interactions and the possibility to follow chemical reactions it may be possible to combine NN-based techniques with empirical FFs. Further applications of reactive FFs include the study of electron or proton transfer reactions. Both processes can be cast within the framework of MS-ARMD(Huang, Buchowiecki, Nagy, Vanicek, & Meuwly, 2014; Karandashev et al., 2017) but alternative techniques have also been employed. Typical applications are the investigation of the change in the solvent structure around metal-complexes(Szymczak, Hofmann, & Meuwly, 2013; Das, Solomon, Hofmann, & Meuwly, 2016; Jin et al., 2016; Das & Meuwly, 2017; Worner et al., 2017) or the spectroscopic signatures accompanying proton transfer.(Vendrell, Gatti, & Meyer, 2007; Bowman, Carrington, & Meyer, 2008; Vendrell, Gatti, & Meyer, 2009; Yang & Meuwly, 2010; Huang et al., 2012; Howard, Kjaergaard, Huang, & Meuwly, 2015; Mackeprang et al., 2016; Xu & Meuwly, 2017), or the energetics of proton transfer in proteins.(Lutz, Tubert-Brohman, Yang, & Meuwly, 2011) A field by itself is the investigation of proton transfer in bulk water for which a myriad of FF-based techniques have been developed.(Schmitt & Voth, 1999; Day, Schmitt, & Voth, 2000; J. Kim, Schmitt, Gruetzmacher, Voth, & Scherer, 2002; Day, Soudackov, Cuma, Schmitt, & Voth, 2002; Voth, 2006; Wolf & Groenhof, 2014; Wiedemair, Hitzenberger, & Hofer, 2015) Finally, modern electronic structure methods may pave the way for *ab initio* MD simulations of large systems on extended time scales. They include hypertensor contractions(Hohenstein, Parrish, & Martinez, 2012) or density renormalization group techniques.(Chan & Sharma, 2011) This may allow to study complex systems in explicit solvent akin to what is currently possible with semiempirical methods such as DFTB3.(Gaus, Cui, & Elstner, 2011)

In summary, using empirical force fields or energies represented using novel numerical tools (RKHS, permutationally invariant polynomials) in reactive MD simulations provides valuable molecular-level insights into a range of physico-chemical processes of practical relevance. An essential aspect of such studies is the validation of the computational model in view of

available experimental data. Based on this, the field of reactive molecular dynamics simulations will continue to make fundamental contributions to elucidating energetic and structural aspects of reactive processes in the gas- and condensed phase.

SIDEBAR: Structural Interpretation of Time Scales

State-of-the art time resolved experiments(Schotte et al., 2003; Hamm, Helbing, & Bredenbeck, 2008; Ghosh, Ostrander, & Zanni, 2017; R. J. D. Miller, 2014; Ischenko, Weber, & Miller, 2017) provide a wealth of information concerning the time scale and, depending on the analysis, the number of elementary steps involved in a physico-chemical process. However, linking different time scales to distinct spatial processes remains a big challenge. Conversely, atomistic simulations contain the full information concerning the spatio-temporal changes in a system. From this time scales and spatial/structural changes of a process can be related. This has been done, e.g., for 2-dimensional infrared spectroscopy(Lee, Carr, Goellner, Hamm, & Meuwly, 2013) or ligand rebinding to a protein.(Soloviov et al., 2016) As such, quantitatively accurate simulations on an ensemble can provide molecular-level insight that is difficult to obtain from experiment alone. However, for non-equilibrium systems (e.g. highly vibrationally excited HSO_2X) a structural interpretation of different time scales observed from the reaction kinetics is complicated. This is because here all elementary processes are characterized by distributions of reaction times.

ACKNOWLEDGEMENTS

References

Abdi, H. (1994). A neural network primer. *J. Biol. Syst.*, *2*(03), 247–281.

Adler, T. B., Knizia, G., & Werner, H.-J. (2007). A simple and efficient CCSD(T)-F12 approximation. *J. Chem. Phys.*, *127*(22), 221106–224100.

Aguado, A., & Paniagua, M. (1992). A new functional form to obtain analytical potentials of triatomic molecules. *J. Chem. Phys.*, *96*(2), 1265–1275.

Ali, M. E., Sanyal, B., & Oppeneer, P. M. (2012). Electronic structure, spin-states, and spin-crossover reaction of Heme-related Fe-porphyrins: A theoretical perspective. *J. Phys. Chem. B*, *116*(20), 5849-5859.

Andrews, P. R., Smith, G. D., & Young, I. G. (1973). Transition-state stabilization and enzymic catalysis. Kinetic and molecular orbital studies of the rearrangement of chorismate to prephenate. *Biochemistry*, *12*(18), 3492–3498.

Aronszajn, N. (1950). Theory of reproducing kernels. *Trans. Amer. Math. Soc.*, *68*(3), 337–404.

Ascenzi, P., Bolognesi, M., & Visca, P. (2007). NO dissociation represents the rate limiting step for O_2-mediated oxidation of ferrous nitrosylated mycobacterium leprae truncated hemoglobin O. *Biochem. Biophys. Res. Commun.*, *357*(3), 809 - 814.

Ascenzi, P., Gullotta, F., Gioia, M., Coletta, M., & Fasano, M. (2011). O_2-mediated oxidation of ferrous nitrosylated human serum heme-albumin is limited by nitrogen monoxide dissociation. *Biochem. Biophys. Res. Commun.*, *406*(1), 112 - 116.

Balakrishnan, N., & Dalgarno, A. (1999). Rate coefficients for NO formation in energetic $N+O_2$ collisions. *Chem. Phys. Lett.*, *302*(5-6), 485-488.

Bang, I.-S., Liu, L., Vazquez-Torres, A., Crouch, M.-L., Stamler, J. S., & Fang, F. C. (2006). Maintenance of nitric oxide and redox homeostasis by the Salmonella flavohemoglobin Hmp. *J. Biol. Chem.*, *281*(38), 28039-28047.

Bartok, A. P., & Csanyi, G. (2015). Gaussian approximation potentials: A brief tutorial introduction. *Int. J. Quant. Chem.*, *115*(16, SI), 1051-1057.

Bauer, P., Barrozo, A., Pung, M., Amrein, B. A., Esguerra, M., Wilson, P. B., . . . Kamerlin, S. C. L. (n.d.). Q6: A comprehensive toolkit for empirical valence bond and related

free energy calculations.

Baulch, D., Cobos, C., Cox, R., Frank, G., P.; Hayman, Just, T., Kerr, J., . . . Warnatz, J. (1994). Evaluated kinetic data for combustion modelling. Supplement I. *J. Phys. Chem. Ref. Data*, *23*, 847-1033.

Behler, J. (2011). Neural network potential-energy surfaces in chemistry: A tool for large-scale simulations. *Phys. Chem. Chem. Phys.*, *13*(40), 17930–17955.

Behler, J., & Parrinello, M. (2007). Generalized neural-network representation of high-dimensional potential-energy surfaces. *Phys. Rev. Lett.*, *98*(14), 146401.

Belyaev, A., Tiukanov, A., & Domcke, W. (2002). Generalized diatomics-in-molecules method for polyatomic anions. *Phys. Rev. A*, *65*(1).

Bettens, R. P., & Collins, M. A. (1999). Learning to interpolate molecular potential energy surfaces with confidence: A Bayesian approach. *J. Chem. Phys.*, *111*(3), 816–826.

Beyer, A. N., Richardson, J. O., Knowles, P. J., Rommel, J., & Althorpe, S. C. (2016). Quantum Tunneling Rates of Gas-Phase Reactions from On-the-Fly Instanton Calculations. *J. Phys. Chem. Lett.*, *7*(21), 4374-4379.

Bishop, C. M. (1995). *Neural networks for pattern recognition*. Oxford university press.

Bokhan, D., Ten-No, S., & Noga, J. (2008). Implementation of the CCSD(T)-F12 method using cusp conditions. *Phys. Chem. Chem. Phys.*, *10*(23), 3320–3326.

Boothroyd, A. I., Keogh, W. J., Martin, P. G., & Peterson, M. R. (1996). A refined H_3 potential energy surface. *J. Chem. Phys.*, *104*(18), 7139–7152.

Bose, D., & Candler, G. (1997). Thermal rate constants of the O_2+N $\rightarrow$ NO+O reaction based on the $A^{2'}$ and $A^{4'}$ potential-energy surfaces. *J. Chem. Phys.*, *107*(16), 6136-6145.

Bowman, J. M., Braams, B. J., Carter, S., Chen, C., Czako, G., Fu, B., . . . *et al.* (2010). Ab-initio-based potential energy surfaces for complex molecules and molecular complexes. *J. Phys. Chem. Lett.*, *1*(12), 1866-1874.

Bowman, J. M., Carrington, T., & Meyer, H.-D. (2008). Variational quantum approaches for computing vibrational energies of polyatomic molecules. *Mol. Phys.*, *106*(16-18), 2145-2182.

Bowman, J. M., Czako, G., & Fu, B. (2011). High-dimensional ab initio potential energy

surfaces for reaction dynamics calculations. *Phys. Chem. Chem. Phys.*, *13*(18), 8094-8111.

Braams, B. J., & Bowman, J. M. (2009). Permutationally invariant potential energy surfaces in high dimensionality. *Int. Rev. Phys. Chem.*, *28*(4), 577–606.

Brickel, S., & Meuwly, M. (2017). OH-Stretching Overtone Induced Dynamics in HSO_3F from Reactive Molecular Dynamics Simulations. *J. Phys. Chem. A*, *121*(27), 5079-5087.

Brooks, B. R., Brooks, C. L., III, Mackerell, A. D., Jr., Nilsson, L., Petrella, R. J., Roux, B., ... Karplus, M. (2009). CHARMM: The Biomolecular Simulation Program. *J. Comput. Chem.*, *30*(10, SI), 1545-1614.

Burkholder, J., Mills, M., & McKeen, S. (2000). Upper limit for the UV absorption cross sections of H_2SO_4. *Geophys. Res. Lett.*, *27*(16), 2493 - 2496.

Carabet, L. A., Guertin, M., Lague, P., & Lamoureux, G. (2017). Mechanism of the Nitric Oxide Dioxygenase Reaction of Mycobacterium tuberculosis Hemoglobin N. *J. Phys. Chem. B*, *121*(37), 8706-8718.

Caridade, P., & Varandas, A. (2004). Dynamics study of the $N(^4S)+O_2$ reaction and its reverse. *J. Phys. Chem. A*, *108*(16), 3556-3564.

Carpenter, B. K., Harvey, J. N., & Glowacki, D. R. (2015). Prediction of enhanced solvent-induced enantioselectivity for a ring opening with a bifurcating reaction path. *Phys. Chem. Chem. Phys.*, *17*(13), 8372-8381.

Cassam-Chenaï, P., & Patras, F. (2008). Symmetry-adapted polynomial basis for global potential energy surfaces-applications to XY_4 molecules. *J. Math. Chem.*, *44*(4), 938–966.

Castro-Palacio, J. C., Bemish, R. J., & Meuwly, M. (2015). Communication: Equilibrium rate coefficients from atomistic simulations: The $O(^3P) + NO(^2\Pi) \rightarrow O_2(^3X\ \Sigma_g^-) + N(^4S)$ reaction at temperatures relevant to the hypersonic flight regime. *J. Chem. Phys.*, *142*(9).

Castro-Palacio, J. C., Nagy, T., Bemish, R. J., & Meuwly, M. (2014). Computational Study of Collisions Between $O(^3P)$ and $NO(^2\Pi)$ at Temperatures Relevant to the Hypersonic Flight Regime. *J. Chem. Phys.*, *141*(16), 164319.

Chan, G. K.-L., & Sharma, S. (2011). The Density Matrix Renormalization Group in Quantum Chemistry. In Leone, SR and Cremer, PS and Groves, JT and Johnson, MA (Ed.), *Ann. Rev. Phys. Chem.* (Vol. 62, p. 465-481).

Chang, Y.-T., & Miller, W. H. (1990). An empirical valence bond model for constructing global potential energy surfaces for chemical reactions of polyatomic molecular systems. *J. Phys. Chem.*, *94*, 5884-5888.

Chase, M. W., Davies, C. A., Downey, J. R., Frurip, D. J., McDonald, R. A., & Syverud, A. N. (1985). JANAF Thermochemical Tables - 3rd edition .1. Al-Co. *J. Phys. Chem. Ref. Data*, *14*(1, 1), 1-926.

Chenoweth, K., van Duin, A. C. T., & Goddard, W. A., III. (2008). ReaxFF reactive force field for molecular dynamics simulations of hydrocarbon oxidation. *J. Phys. Chem. A*, *112*(5), 1040-1053.

Claisen, L. (1912). Über Umlagerung von Phenol-allyläthern in C-Allyl-phenole. *Chem. Ber.*, *45*(3), 3157–3166.

Clark, J. W. (1999). Neural networks: New tools for modelling and data analysis in science. In *Scientific applications of neural nets* (pp. 1–96). Springer.

Clark, T., Garnett, S. H., & Kistiak, G. B. (1969). Reaction of carbon dioxide with atomic oxygen and the dissociation of carbon dioxide in shock waves. *J. Chem. Phys.*, *51*, 2885-2891.

Collins, M. A. (2002). Molecular potential-energy surfaces for chemical reaction dynamics. *Theor. Chem. Acc.*, *108*(6), 313–324.

Cornelius, P., Hochstrasser, R., & Steele, A. (1983). Ultrafast relaxation in picosecond photolysis of nitrosylhemoglobin. *J. Mol. Biol.*, *163*(1), 119-128.

Coulson, C. A., & Danielsson, U. (1954). Ionic and covalent contributions to the hydrogen bond .1. *Ark. Fys.*, *8*, 239-244.

Crim, F. (1993). Vibrationally mediated photodissociation - exploring excited-state surfaces and controlling decomposition pathways. *Ann. Rev. Phys. Chem.*, *44*, 397-428.

Cui, Q. (2016). Perspective: Quantum mechanical methods in biochemistry and biophysics. *J. Chem. Phys.*, *145*(14).

Danielsson, J., & Meuwly, M. (2008). Atomistic simulation of adiabatic reactive processes

based on multi-state potential energy surfaces. *J. Chem. Theo. Comp.*, *4*, 1083.

Das, A. K., & Meuwly, M. (2017). Hydration Control Through Intramolecular Degrees of Freedom: Molecular Dynamics of [Cu(II)(Imidazole)$_4$]. *J. Phys. Chem. B*, *121*(38), 9024-9031.

Das, A. K., & Meuwly, M. (2018). Kinetics and Structural Interpretation of Competitive Ligand Binding for NO Dioxygenation in Truncated Hemoglobin N. *Angew. Chem. Intern. Ed.*, *57*(13), 3509-3513.

Das, A. K., Solomon, R. V., Hofmann, F., & Meuwly, M. (2016). Inner-Shell Water Rearrangement Following Photoexcitation of Tris(2,2'-bipyridine)iron(II). *J. Phys. Chem. B*, *120*(1), 206-216.

Dawes, R., Thompson, D. L., Wagner, A. F., & Minkoff, M. (2008). Interpolating moving least-squares methods for fitting potential energy surfaces: A strategy for efficient automatic data point placement in high dimensions. *J. Chem. Phys.*, *128*(8), 084107.

Day, T., Schmitt, U., & Voth, G. (2000). The mechanism of hydrated proton transport in water. *J. Am. Chem. Soc.*, *122*(48), 12027-12028.

Day, T., Soudackov, A., Cuma, M., Schmitt, U., & Voth, G. (2002). A second generation multistate empirical valence bond model for proton transport in aqueous systems. *J. Chem. Phys.*, *117*(12), 5839-5849.

Defazio, P., Petrongolo, C., Gray, S., & Oliva, C. (2001). Wave packet dynamics of the $N(^4S)+O_2(X^3\Sigma_g^-) \rightarrow NO(X^2\Pi)+O(^3P)$ reaction on the X^2A' potential energy surface. *J. Chem. Phys.*, *115*(7), 3208-3214.

Defazio, P., Petrongolo, C., Oliva, C., Gonzalez, M., & Sayos, R. (2002). Quantum dynamics of the $N(^4S)+O_2$ reaction on the X^2A' and a^4A' surfaces: Reaction probabilities, cross sections, rate constants, and product distributions. *J. Chem. Phys.*, *117*(8), 3647-3655.

Denis-Alpizar, O., Bemish, R. J., & Meuwly, M. (2017). Reactive collisions for $NO(^2\Pi)$ + $N(^4S)$ at temperatures relevant to the hypersonic flight regime. *Phys. Chem. Chem. Phys.*, *19*(3), 2392-2401.

Denis-Alpizar, O., Unke, O. T., Bemish, R. J., & Meuwly, M. (2017). Quantum and quasiclassical trajectory studies of rotational relaxation in Ar-N_2^+ collisions. *Phys. Chem. Chem. Phys.*, *19*(41), 27945-27951.

Dhont, G., van Lenthe, J., Groenenboom, G., & van der Avoird, A. (2005). Ab initio calculation of the NH($^3\Sigma^-$)-NH($^3\Sigma^-$) interaction potentials in the quintet, triplet, and singlet states. *J. Chem. Phys.*, *123*(18).

Dirac, P. (1929). Quantum mechanics of many-electron systems. *Proc. R. Soc. Lond. Ser. A*, *123*(792), 714-733.

Donaldson, D., Frost, G., Rosenlof, K., & Tuck, V., A.F. Vaida. (1997). Atmospheric radical production by excitation of vibrational overtones via absorption of visible light. *Geophys. Res. Lett.*, *24*(21), 2651 - 2654.

Doyle, M. P., & Hoekstra, J. W. (1981). Oxidation of nitrogen oxides by bound dioxygen in hemoproteins. *J. Inorg. Biochem.*, *14*(4), 351-358.

Duarte, F., & Kamerlin, S. E. (2017). *From physical chemistry to chemical biology: Theory and applications of the empirical valence bond approach.* Wiley.

Duchovic, R. J., Volobuev, Y. L., Lynch, G. C., Truhlar, D. G., Allison, T. C., Wagner, A. F., . . . Corchado, J. C. (2002). Potlib 2001: A potential energy surface library for chemical systems. *Comput. Phys. Commun.*, *144*(2), 169–187.

Eich, R. F., Li, T., Lemon, D. D., Doherty, D. H., Curry, S. R., Aitken, J. F., . . . Olson, J. S. (1996). Mechanism of NO-induced oxidation of Myoglobin and Hemoglobin. *Biochem.*, *35*, 6976-6983.

El Hage, K., Brickel, S., Hermelin, S., Gaulier, G., Schmidt, C., Bonacina, L., . . . Meuwly, M. (2017). Implications of short time scale dynamics on long time processes. *Struct. Dyn.*, *4*(6).

Ellison, F. O. (1963). A Method of Diatomics in Molecules. 1. General Theory and Application to H_2O. *J. Am. Chem. Soc.*, *85*, 3540-3544.

Esposito, F., & Armenise, I. (2017). Reactive, Inelastic, and Dissociation Processes in Collisions of Atomic Oxygen with Molecular Nitrogen. *J. Phys. Chem. A*, *121*(33), 6211-6219.

Firman, T. K., & Landis, C. R. (2001). Valence bond concepts applied to the molecular mechanics description of molecular shapes. 4. Transition metals with pi-bonds. *J. Am. Chem. Soc.*, *123*(47), 11728–11742.

Florian, J. (2002). Comments on molecular mechanics for chemical reactions. *J. Phys.*

Chem. A, *106*, 5046-5047.

Franke, R., & Nielson, G. (1980). Smooth interpolation of large sets of scattered data. *Int. J. Numer. Meth. Eng.*, *15*(11), 1691–1704.

Franzen, S. (2002). Spin-dependent mechanism for diatomic ligand binding to heme. *Proc. Natl. Acad. Sci.*, *99*(26), 16754-16759.

Gamallo, P., Gonzalez, M., & Sayos, R. (2003). Ab initio study of the two lowest triplet potential energy surfaces involved in the $N(^4S)+NO\ (X^2\Pi)$ reaction. *J. Chem. Phys.*, *118*(23), 10602-10610.

Gaus, M., Cui, Q., & Elstner, M. (2011). DFTB3: Extension of the Self-Consistent-Charge Density-Functional Tight-Binding Method (SCC-DFTB). *J. Chem. Theo. Comp.*, *7*(4), 931-948.

Ghosh, A., Ostrander, J. S., & Zanni, M. T. (2017). Watching Proteins Wiggle: Mapping Structures with Two Dimensional Infrared Spectroscopy. *Chem. Rev.*, *117*(16, SI), 10726-10759.

Gilibert, M., Aguilar, A., Gonzalez, M., & Sayos, R. (1993). Quasiclassical Trajectory Study of the $N(^4S_u)+O_2(X\ ^3\Sigma_g^-) \rightarrow NO(X\ ^2\Pi)+O(^3P_g)$ Atmospheric Reaction on the ^2A' Ground Potential Energy Surface Employing an Analytical Sorbie-Murrell Potential. *Chem. Phys.*, *172*(1), 99-115.

Gilibert, M., Gimenez, X., Gonzalez, M., Sayos, R., & Aguilar, A. (1995). A Comparison between Experimental, Quantum and Quasi-Classical Properties for the $N(^4S)+O_2(X^3\Sigma_g) \rightarrow NO(X^2\Pi)+O(^3P)$ Reaction. *Chem. Phys.*, *191*(1-3), 1-15.

Gladwin, M., Lancaster, J., Freeman, B., & Schechter, A. (2003). Nitric oxide's reactions with hemoglobin: a view through the SNO-storm. *Nature Medicine*, *9*(5), 496-500.

Glowacki, D. R., Orr-Ewing, A. J., & Harvey, J. N. (2015). Non-equilibrium reaction and relaxation dynamics in a strongly interacting explicit solvent: $F + CD_3CN$ treated with a parallel multi-state EVB model. *J. Chem. Phys.*, *143*(4).

Glowacki, D. R., Rodgers, W. J., Shannon, R., Robertson, S. H., & Harvey, J. N. (2017). Reaction and relaxation at surface hotspots: using molecular dynamics and the energy-grained master equation to describe diamond etching. *Proc. Roy. Soc. Lond.*, *375*(2092).

Glowacki, D. R., Rose, R. A., Greaves, S. J., Orr-Ewing, A. J., & Harvey, J. N. (2011). Ultrafast energy flow in the wake of solution-phase bimolecular reactions. *Nuovo Cim.*, *3*(11), 850-855.

Golub, G. H., & Kahan, W. (1965). Calculating the singular values and pseudo-inverse of a matrix. *J. Soc. Ind. Appl. Math.: Ser. B, Num. Analysis*, *2*, 205.

Golub, G. H., & Van Loan, C. F. (2012). *Matrix computations* (Vol. 3). JHU Press Baltimore.

Gonzalez, M., Oliva, C., & Sayos, R. (2002). The lowest doublet and quartet potential energy surfaces involved in the $N(^4S)+O_2$ reaction. II. Ab initio study of the C_2v-symmetry insertion mechanism. *J. Chem. Phys.*, *117*(2), 680-692.

Gordon, S., & McBride, B. J. (1996). Computer program for calculation of complex chemical equilibrium compositions and applications. *NASA Reference Publication*, 1311.

Greaves, S. J., Rose, R. A., Oliver, T. A. A., Glowacki, D. R., Ashfold, M. N. R., Harvey, J. N., ... Orr-Ewing, A. J. (2011). Vibrationally Quantum-State-Specific Reaction Dynamics of H Atom Abstraction by CN Radical in Solution. *Science*, *331*(6023), 1423-1426.

Hamm, P., Helbing, J., & Bredenbeck, J. (2008). Two-dimensional infrared spectroscopy of photoswitchable peptides. *Ann. Rev. Phys. Chem.*, *59*, 291-317.

Handley, C. M., & Popelier, P. L. (2010). Potential energy surfaces fitted by artificial neural networks. *J. Phys. Chem. A*, *114*(10), 3371–3383.

Hangelbroek, T., & Ron, A. (2010). Nonlinear approximation using Gaussian kernels. *J. Func. Analysis*, *259*, 203.

Hansen, K., Biegler, F., Ramakrishnan, R., Pronobis, W., Von Lilienfeld, O. A., Müller, K.-R., & Tkatchenko, A. (2015). Machine learning predictions of molecular properties: Accurate many-body potentials and nonlocality in chemical space. *J. Phys. Chem. Lett*, *6*(12), 2326–2331.

Hansen, K., Montavon, G., Biegler, F., Fazli, S., Rupp, M., Scheffler, M., ... Muller, K.-R. (2013). Assessment and validation of machine learning methods for predicting molecular atomization energies. *J. Chem. Theory Comput.*, *9*(8), 3404–3419.

Haykin, S. S. (2009). *Neural networks and learning machines* (Vol. 3). Pearson Upper Saddle

River, NJ, USA:.

Helbing, J., Bonacina, L., Pietri, R., Bredenbeck, J., Hamm, P., van Mourik, F., ... López-Garriga, J. (2004). Time-resolved visible and infrared study of the cyano complexes of myoglobin and of hemoglobin I from Lucina Pectinata. *Biophys. J.*, *87*, 1881.

Herold, S., Exner, M., & Nauser, T. (2001). Kinetic and mechanistic studies of the no·-mediated oxidation of oxymyoglobin and oxyhemoglobin. *Biochem.*, *40*(11), 3385-3395.

Hess, B., Kutzner, C., van der Spoel, D., & Lindahl, E. (2008). GROMACS 4: Algorithms for highly efficient, load-balanced, and scalable molecular simulation. *J. Chem. Theo. Comp.*, *4*(3), 435-447.

Hestenes, M. R. (1958). Inversion of matrices by biorthogonalization and related results. *J. Soc. Ind. Appl. Math.*, *6*, 52.

Hinton, G., Deng, L., Yu, D., Dahl, G. E., Mohamed, A.-R., Jaitly, N., ... Sainath, T. N. (2012). Deep neural networks for acoustic modeling in speech recognition: The shared views of four research groups. *IEEE Signal Process. Mag.*, *29*(6), 82–97.

Hintze, P. E., Kjaergaard, H. G., Vaida, V., & Burkholder, J. B. (2003). Vibrational and electronic spectroscopy of sulfuric acid vapor. *J. Chem. Phys.*, *107*(8), 1112 - 1118.

Ho, T.-S., Hollebeek, T., Rabitz, H., Harding, L. B., & Schatz, G. C. (1996). A Global H_2O Potential Energy Surface for the Reaction $O(^1D) + H_2 \rightarrow OH + H$. *J. Chem. Phys.*, *105*(23), 10472–10486.

Ho, T.-S., & Rabitz, H. (1996). A general method for constructing multidimensional molecular potential energy surfaces from ab initio calculations. *J. Chem. Phys.*, *104*(7), 2584–2597.

Hofmann, T., Schölkopf, B., & Smola, A. J. (2008). Kernel methods in machine learning. *Ann. Stat.*, 1171–1220.

Hohenstein, E. G., Parrish, R. M., & Martinez, T. J. (2012). Tensor hypercontraction density fitting. I. Quartic scaling second- and third-order Møller-Plesset perturbation theory. *J. Chem. Phys.*, *137*(4).

Hollebeek, T., Ho, T.-S., & Rabitz, H. (1997). A fast algorithm for evaluating multidimensional potential energy surfaces. *J. Chem. Phys.*, *106*(17), 7223–7227.

Hollebeek, T., Ho, T.-S., & Rabitz, H. (1999). Constructing multidimensional molecular potential energy surfaces from ab initio data. *Annu. Rev. Phys. Chem.*, *50*(1), 537–570.

Hong, G., Rosta, E., & Warshel, A. (2006). Using the constrained DFT approach in generating diabatic surfaces and off diagonal empirical valence bond terms for modeling reactions in condensed phases. *J. Phys. Chem. B*, *110*, 19570-19574.

Howard, D. L., Kjaergaard, H. G., Huang, J., & Meuwly, M. (2015). Infrared and Near-Infrared Spectroscopy of Acetylacetone and Hexafluoroacetylacetone. *J. Phys. Chem. A*, *119*(29), 7980-7990.

Huang, J., Buchowiecki, M., Nagy, T., Vanicek, J., & Meuwly, M. (2014). Kinetic isotope effect in malonaldehyde determined from path integral Monte Carlo simulations. *Phys. Chem. Chem. Phys.*, *16*(1), 204-211.

Huang, J., Haeussinger, D., Gellrich, U., Seiche, W., Breit, B., & Meuwly, M. (2012). Hydrogen-Bond and Solvent Dynamics in Transition Metal Complexes: A Combined Simulation and NMR-Investigation. *J. Phys. Chem. B*, *116*(49), 14406-14415.

Hutson, J. M. (1990). Intermolecular Forces from the Spectroscopy of Van der Waals Molecules. *Ann. Rev. Phys. Chem.*, *41*, 123-154.

Hutson, J. M. (1992). Vibrational Dependence of the Anisotropic Intermolecular Potential of Ar-HF. *J. Chem. Phys.*, *96*(9), 6752-6767.

Ionascu, D., Gruia, F., Ye, X., Yu, A., Rosca, F., Demidov, C. B. A., ... Champion, P. M. (2005). Temperature-dependent studies of NO recombination to heme and heme proteins. *J. Am. Chem. Soc.*, *127*, 16921–16934.

Ischenko, A. A., Weber, P. M., & Miller, R. J. D. (2017). Capturing Chemistry in Action with Electrons: Realization of Atomically Resolved Reaction Dynamics. *Chem. Rev.*, *117*(16, SI), 11066-11124.

Ischtwan, J., & Collins, M. A. (1994). Molecular potential energy surfaces by interpolation. *J. Chem. Phys.*, *100*(11), 8080–8088.

Jensen, K. P., & Ryde, U. (2004). How O_2 binds to heme: Reasons for rapid binding and spin inversion. *J. Biol. Chem.*, *279*(15), 14561-14569.

Jiang, B., Li, J., & Guo, H. (2016). Potential energy surfaces from high fidelity fitting of

ab initio points: the permutation invariant polynomial-neural network approach. *Int. Rev. Phys. Chem.*, *35*(3), 479–506.

Jin, H., Goyal, P., Das, A. K., Gaus, M., Meuwly, M., & Cui, Q. (2016). Copper Oxidation/Reduction in Water and Protein: Studies with DFTB3/MM and VALBOND Molecular Dynamics Simulations. *J. Phys. Chem. B*, *120*(8), 1894-1910.

Johnston, H. S., & Parr, C. (1963). Activation Energies from Bond energies. I. Hydrogen Transfer Reactions. *J. Am. Chem. Soc.*, *85*, 2544-2551.

Jordan, M. J., Thompson, K. C., & Collins, M. A. (1995a). Convergence of Molecular Potential Energy Surfaces by Interpolation: Application to the OH + $H_2 \rightarrow H_2O$ + H Reaction. *J. Chem. Phys.*, *102*(14), 5647–5657.

Jordan, M. J., Thompson, K. C., & Collins, M. A. (1995b). The utility of higher order derivatives in constructing molecular potential energy surfaces by interpolation. *J. Chem. Phys.*, *103*(22), 9669–9675.

Kamerlin, S. C. L., Cao, J., Rosta, E., & Warshel, A. (2009). On Unjustifiably misrepresenting the EVB approach while simultaneously adopting it. *J. Phys. Chem. B*, *113*, 10905-10915.

Karandashev, K., Xu, Z.-H., Meuwly, M., Vanicek, J., & Richardson, J. O. (2017). Kinetic isotope effects and how to describe them. *Struct. Dyn.*, *4*(6).

Karplus, M., Sharma, R., & Porter, R. (1964). Dynamics of reactive collisions: $H+H_2$ exchange reaction. *J. Chem. Phys.*, *40*(7), 2033-2034.

Kast, P., Asif-Ullah, M., & Hilvert, D. (1996). Is chorismate mutase a prototypic entropy trap? - Activation parameters for the Bacillus subtilis enzyme. *Tetrahedron Lett.*, *37*(16), 2691–2694.

Kepp, K. P. (2013). O_2 binding to heme is strongly facilitated by near-degeneracy of electronic states. *Chem. Phys. Chem.*, *14*(15), 3551–3558.

Kern, J., Tran, R., Alonso-Mori, R., Koroidov, S., Echols, N., Hattne, J., ... Yachandra, V. K. (2014). Taking snapshots of photosynthetic water oxidation using femtosecond X-ray diffraction and spectroscopy. *Nat. Comm.*, *5*.

Kim, J., Park, J., Lee, T., & Lim, M. (2012). Dynamics of Geminate Rebinding of NO with Cytochrome c in Aqueous Solution Using Femtosecond Vibrational Spectroscopy. *J.*

Phys. Chem. B, *116*(46), 13663-13671.

Kim, J., Schmitt, U., Gruetzmacher, J., Voth, G., & Scherer, N. (2002). The vibrational spectrum of the hydrated proton: Comparison of experiment, simulation, and normal mode analysis. *J. Chem. Phys.*, *116*(2), 737-746.

Kim, S., Jin, G., & Lim, M. (2004). Dynamics of Geminate Recombination of NO with Myoglobin in Aqueous Solution Probed by Femtosecond Mid-IR Spectroscopy. *J. Phys. Chem. B*, *108*(52), 20366.

Knizia, G., Adler, T. B., & Werner, H.-J. (2009). Simplified CCSD(T)-F12 methods: Theory and benchmarks. *J. Chem. Phys.*, *130*(5), 054104.

Koebke, K. J., Waletzko, M. T., & Pacheco, A. A. (2016). Direct Monitoring of the Reaction between Photochemically Generated Nitric Oxide and Mycobacterium tuberculosis Truncated Hemoglobin N Wild Type and Variant Forms: An Assessment of Computational Mechanistic Predictions. *Biochem.*, *55*(4), 686-696.

Kohonen, T. (1988). An introduction to neural computing. *Neural Netw.*, *1*(1), 3–16.

Kolb, B., Marshall, P., Zhao, B., Jiang, B., & Guo, H. (2017, APR 6). Representing Global Reactive Potential Energy Surfaces Using Gaussian Processes. *J. Phys. Chem. A*, *121*(13), 2552-2557.

Kollau, A., Russwurm, M., Neubauer, A., Rechberger, G., Schmidt, K., Koesling, D., . . . Mayer, B. (2016, APR 1). Scavenging of nitric oxide by hemoglobin in the tunica media of porcine coronary arteries. *Nitric Oxide Biol. Chem.*, *54*, 8-14.

Kruglik, S. G., Yoo, B.-K., Franzen, S., Vos, M. H., Martin, J.-L., & Negrerie, M. (2010). Picosecond primary structural transition of the heme is retarded after nitric oxide binding to heme proteins. *Proc. Natl. Acad. Sci.*, *107*, 13678.

Kulik, H. J., Zhang, J., Klinman, J. P., & Martinez, T. J. (2016). How Large Should the QM Region Be in QM/MM Calculations? The Case of Catechol O-Methyltransferase. *J. Phys. Chem. B*, *120*(44), 11381-11394.

Lammers, S., Lutz, S., & Meuwly, M. (2008). Reactive force fields for proton transfer dynamics. *J. Comput. Chem.*, *29*, 1048-1063.

Lancaster, P., & Salkauskas, K. (1981). Surfaces generated by moving least squares methods. *Math. Comp.*, *37*(155), 141–158.

Landis, C. R., Cleveland, T., & Firman, T. K. (1998, March). Valence Bond Concepts Applied to the Molecular Mechanics Description of Molecular Shapes. 3. Applications to Transition Metal Alkyls and Hydrides. *J. Am. Chem. Soc.*, *120*(11), 2641–2649. Retrieved from http://pubs.acs.org/doi/abs/10.1021/ja9734859 doi: 10.1021/ja9734859

Law, M. M., & Hutson, J. M. (1997). I-NoLLS: A Program for Interactive Nonlinear Least-Squares Fitting of the Parameters of Physical Models. *Comput. Phys. Commun.*, *102*(1), 252–268.

Lawrence, S., Giles, C. L., Tsoi, A. C., & Back, A. D. (1997). Face recognition: A convolutional neural-network approach. *IEEE Trans. Neural Netw.*, *8*(1), 98–113.

Lee, M. W., Carr, J. K., Goellner, M., Hamm, P., & Meuwly, M. (2013). 2D IR spectra of cyanide in water investigated by molecular dynamics simulations. *J. Chem. Phys.*, *139*(5).

LeRoy, R. J., & Hutson, J. M. (1987). Improved Potential Energy Surfaces for the Interaction of H_2 with Ar, Kr, and Xe . *J. Chem. Phys.*, *86*(2), 837-853.

Li, D., Keresztes, I., Hopson, R., & Williard, P. G. (2009). Characterization of Reactive Intermediates by Multinuclear Diffusion-Ordered NMR Spectroscopy (DOSY). *Acc. Chem. Res.*, *42*(2), 270-280.

Li, H., Elber, R., & Straub, J. E. (1993). Molecular-dynamics simulation of NO recombination to myoglobin mutants. *J. Biol. Chem.*, *268*, 17908-17916.

Li, J., Wang, Y., Jiang, B., Ma, J., Dawes, R., Xie, D., . . . Guo, H. (2012). Communication: A chemically accurate global potential energy surface for the $HO + CO \rightarrow H + CO_2$ reaction. *J. Chem. Phys.*, *136*(4), 041103.

Lim, M. H., Jackson, T. A., & Anfinrud, P. A. (1993). Nonexponential Protein Relaxation - Dynamics of Conformational Change in Myoglobin. *Proc. Natl. Acad. Sci.*, *90*(12), 5801-5804.

Lin, W., Meana-Paneda, R., Varga, Z., & Truhlar, D. G. (2016). A quasiclassical trajectory study of the $N_2(X^1\Sigma) + O(^3P) \rightarrow NO(Xi^2\Pi) + N(^4S)$ reaction. *J. Chem. Phys.*, *144*(23).

Lin, W., Varga, Z., Song, G., Paukku, Y., & Truhlar, D. G. (2016). Global triplet potential

energy surfaces for the $N_2(X^1\Sigma) + O(^3P) \rightarrow NO(X^2\Pi) + N(^4S)$ reaction. *J. Chem. Phys.*, *144*(2).

London, F. (1929). Quantum mechanical interpretation of the process of activation. *Z. Elektrochem.*, *35*, 552-555.

Ludwig, J., Vlachos, D. G., van Duin, A. C. T., & Goddard III, W. A. (2006). Dynamics of the dissociation of hydrogen on stepped platinum surfaces using the ReaxFF reactive force field. *J. Phys. Chem. B*, *110*, 4274-4282.

Lundberg, J. O., Gladwin, M. T., Ahluwalia, A., Benjamin, N., Bryan, N. S., Butler, A., ... Weitzberg, E. (2009). Nitrate and nitrite in biology, nutrition and therapeutics. *Nat. Chem. Biol.*, *5*(12), 865-869.

Lutz, S., Tubert-Brohman, I., Yang, Y., & Meuwly, M. (2011). Water-assisted Proton Transfer in Ferredoxin I. *J. Biol. Chem.*, *286*(27), 23679-23687.

Ma, J., Huo, S., & Straub, J. (1997). Molecular dynamics simulation study of the B-states of solvated carbon monoxymyoglobin. *J. Am. Chem. Soc.*, *119*(10), 2541-2551.

Ma, J.-J., Chen, M.-D., Cong, S.-L., & Han, K.-L. (2006). Stereodynamics study of the $N(^4S)+O_2(X^3\Sigma_g^-) \rightarrow O(^3P)+NO(X^2\Pi)$ reaction. *Chem. Phys.*, *327*(2-3), 529-535.

Mackeprang, K., Xu, Z.-H., Maroun, Z., Meuwly, M., & Kjaergaard, H. G. (2016). Spectroscopy and dynamics of double proton transfer in formic acid dimer. *Phys. Chem. Chem. Phys.*, *18*(35), 24654-24662.

Malshe, M., Narulkar, R., Raff, L., Hagan, M., Bukkapatnam, S., Agrawal, P., & Komanduri, R. (2009). Development of generalized potential-energy surfaces using many-body expansions, neural networks, and moiety energy approximations. *J. Chem. Phys.*, *130*(18), 184102.

Manzhos, S., & Carrington Jr, T. (2006). A random-sampling high dimensional model representation neural network for building potential energy surfaces. *J. Chem. Phys.*, *125*(8), 084109.

Manzhos, S., & Carrington Jr, T. (2007). Using redundant coordinates to represent potential energy surfaces with lower-dimensional functions. *J. Chem. Phys.*, *127*(1), 014103.

Martin, A., & Boyd, I. (2011). CFD Implementation of a novel carbon-phenolic-in-air chemistry model for atmospheric re-entry [Conference Paper]. In *49th AIAA Aerospace*

Sciences Meeting including the New Horizons Forum and Aerospace Exposition (p. 18 pp.). (49th AIAA Aerospace Sciences Meeting including the New Horizons Forum and Aerospace Exposition, 4-7 Jan. 2011, Orlando, FL, USA)

Mas, E., Bukowski, R., Szalewicz, K., Groenenboom, G., Wormer, P., & van der Avoird, A. (2000). Water pair potential of near spectroscopic accuracy. I. Analysis of potential surface and virial coefficients. *J. Chem. Phys.*, *113*(16), 6687-6701.

Mayneris, J., Gonzalez, M., & Gray, S. K. (2008). Real wavepacket code for ABC plus D $\rightarrow$ AB plus CD reactive scattering. *Comput. Phys. Commun.*, *179*(10), 741-747.

McBride, B., Zehe, M., & Gordon, S. (2002). NASA Glenn Coefficients for Calculating Thermodynamic Properties of Individual Species. *NASA report TP-2002-211556*.

McCulloch, W. S., & Pitts, W. (1943). A logical calculus of the ideas immanent in nervous activity. *Bull. Math. Biophys.*, *5*(4), 115–133.

Merchant, K. A., Noid, W. G., Thompson, D. E., Akiyama, R., Loring, R. F., & Fayer, M. D. (2003). Structural assignments and dynamics of the A substates of MbCO: spectrally resolved vibrational echo experiments and molecular dynamics simulations. *J. Phys. Chem. B*, *107*, 4-7.

Meuwly, M., Becker, O., Stote, R., & Karplus, M. (2002). NO rebinding to Myoglobin: A reactive molecular dynamics study. *Biophys. Chem.*, *89*, 183-207.

Meuwly, M., & Hutson, J. (1999b). The potential energy surface and near-dissociation states of He-H_2^+. *J. Chem. Phys.*, *110*(7), 3418-3427.

Meuwly, M., & Hutson, J. M. (1999a). Morphing *ab initio* potentials: A systematic study of NeHF. *J. Chem. Phys.*, *110*(17), 8338-8347.

Miller, R. J. D. (2014). Femtosecond Crystallography with Ultrabright Electrons and X-rays: Capturing Chemistry in Action. *Science*, *343*(6175), 1108-1116.

Miller, Y., & Gerber, R. B. (2006). Dynamics of vibrational overtone excitations of H_2SO_4, H_2SO_4-H_2O: Hydrogen-hopping and photodissociation processes. *J. Am. Chem. Soc.*, *128*(30), 9594 - 9595.

Millikan, R. C., & White, D. R. (1963). Systematics of vibrational relaxation. *J. Chem. Phys.*, *39*(12), 3209.

Mishra, S., & Meuwly, M. (2010). Atomistic Simulation of NO Dioxygenation in Group I

Truncated Hemoglobin. *J. Am. Chem. Soc.*, *132*(9), 2968-2982.

Montavon, G., Rupp, M., Gobre, V., Vazquez-Mayagoitia, A., Hansen, K., Tkatchenko, A., ... Von Lilienfeld, O. A. (2013). Machine learning of molecular electronic properties in chemical compound space. *New J. Phys.*, *15*(9), 095003.

Nagy, T., Yosa Reyes, J., & Meuwly, M. (2014). Multisurface adiabatic reactive molecular dynamics. *J. Chem. Theo. Comp.*, *10*(4), 1366-1375.

Nguyen, K. A., Rossi, I., & Truhlar, D. G. (1995). A dual-level shepard interpolation method for generating potential energy surfaces for dynamics calculations. *J. Chem. Phys.*, *103*(13), 5522–5530.

Nienhaus, K., Lutz, S., Meuwly, M., & Nienhaus, G. U. (2013). Reaction-pathway selection in the structural dynamics of a heme protein. *Chem. Eur. J.*, *19*, 3558-3562.

Nutt, D. R., & Meuwly, M. (2006). Studying reactive processes with classical dynamics: Rebinding dynamics in MbNO. *Biophys. J.*, *90*, 1191-1201.

Olson, J. A., & Garrison, B. J. (1984). Diatomics in Molecules - a Simplified Approach. *J. Chem. Phys.*, *81*(3), 1355-1359.

Pacher, P., Beckman, J. S., & Liaudet, L. (2007). Nitric oxide and peroxynitrite in health and disease. *Physiol. Rev.*, *87*(1), 315-424.

Paukku, Y., Yang, K. R., Varga, Z., & Truhlar, D. G. (2013). Global Ab Initio Ground-State Potential Energy Surface of N_4. *J. Chem. Phys.*, *139*(4), 044309.

Pauling, L. (1947). Atomic radii and interatomic distances in metals. *J. Am. Chem. Soc.*, *69*, 542-553.

Peng, T., Zhang, D., Wang, D., Li, Y., & Zhang, J. (2000). Dynasol: A visual quantum dynamics package. *Comput. Phys. Commun.*, *128*(1-2), 492-495.

Penney, W. (1937). The electronic structure of some polyenes and aromatic molecules. III. Bonds of fractional order by the pair method. *Proc. Roy. Soc. Lond.*, *158*(A894), 0306-0324.

Petrich, J. W., Lambry, J. C., Kuczera, K., Karplus, M., Poyart, C., & Martin, J. L. (1991). Ligand binding and protein relaxation in heme proteins: a room temperature analysis of nitric oxide geminate recombination. *Biochem.*, *30*(16), 3975.

Poole, R., & Hughes, M. (2000). New functions for the ancient globin family: bacterial

responses to nitric oxide and nitrosative stress. *Mol. Microbiol.*, *36*(4), 775-783.

Porter, R., & Karplus, M. (1964). Potential Energy Surface for H3. *J. Chem. Phys.*, *40*(4), 1105-1115.

Ramakrishnan, R., Dral, P. O., Rupp, M., & Von Lilienfeld, O. A. (2014). Quantum chemistry structures and properties of 134 kilo molecules. *Sci. Data*, *1*, 140022.

Ripley, B. D. (2007). *Pattern recognition and neural networks.* Cambridge university press.

Robinson, T. W., Schofield, D. P., & Kjaergaard, H. G. (2003). High level ab initio studies of the excited states of sulfuric acid and sulfur trioxide. *J. Chem. Phys.*, *118*(7226), 7226 - 7232.

Roche, C., Ernesti, A., Hutson, J., & Dickinson, A. (1996). Evaluation of existing potential energy surfaces for CO_2-Ar: Pressure broadening and high-resolution spectroscopy of van der Waals complexes. *J. Chem. Phys.*, *104*(6), 2156-2166.

Rosen, J., & Hofmann, D. (1983). Unusual behavior in the condensation nuclei concentration at 30 km. *J. Geophys. Res.*, *88*(6), 3725 - 3731.

Roston, D., Demapan, D., & Cui, Q. (2016). Leaving Group Ability Observably Affects Transition State Structure in a Single Enzyme Active Site. *J. Am. Chem. Soc.*, *138*(23), 7386-7394.

Rupp, M. (2015). Machine learning for quantum mechanics in a nutshell. *Int. J. Quantum Chem.*, *115*(16), 1058–1073.

Rupp, M., Tkatchenko, A., Müller, K.-R., & Von Lilienfeld, O. A. (2012). Fast and accurate modeling of molecular atomization energies with machine learning. *Phys. Rev. Lett.*, *108*(5), 058301.

Russo, M. F., Jr., & van Duin, A. C. T. (2011). Atomistic-scale simulations of chemical reactions: Bridging from quantum chemistry to engineering. *Nucl. Instr. Meth. Phys. Res. B*, *269*(14), 1549-1554.

Sato, S. (1955a). On a new method of drawing the potential energy surface. *J. Chem. Phys.*, *23*, 592-593.

Sato, S. (1955b). Potential energy surface of the system of three atoms. *J. Chem. Phys.*, *23*, 2465-2466.

Schatz, G., & Kuppermann, A. (1976). Quantum-Mechanical Scattering for 3-Dimensional

Atom plus Diatom Systems: 2 Accurate Cross-Sections for H+H_2. *J. Chem. Phys.*, *65*(11), 4668-4692.

Schlegel, H. B., & Sonnenberg, J. L. (2006). Empirical valence-bond models for reactive potential energy surfaces using distributed Gaussians. *J. Chem. Theo. Comp.*, *2*(4), 905-911.

Schmid, M., Das, A. K., Landis, C. R., & Meuwly, M. (2018). Multi-State VALBOND for Atomistic Simulations of Hypervalent Molecules, Metal Complexes and Reactions. *J. Chem. Theo. Comp.*, *in print*.

Schmitt, U., & Voth, G. (1998). Multistate empirical valence bond model for proton transport in water. *J. Phys. Chem. B*, *102*(29), 5547-5551.

Schmitt, U., & Voth, G. (1999). The computer simulation of proton transport in water. *J. Chem. Phys.*, *111*(20), 9361-9381.

Schölkopf, B., Herbrich, R., & Smola, A. J. (2001). A generalized representer theorem. In *International conference on computational learning theory* (pp. 416–426). Springer Berlin Heidelberg.

Schotte, F., Lim, M., Jackson, T. A., Smirnov, A. V., Soman, J., Olson, J. S., . . . Anfinrud, P. A. (2003). Watching a protein as it functions with 150 ps time-resolved X-ray crystallography. *Science*, *300*, 1944-1947.

Schütt, K. T., Arbabzadah, F., Chmiela, S., Müller, K. R., & Tkatchenko, A. (2017). Quantum-chemical insights from deep tensor neural networks. *Nat. Commun.*, *8*, 13890.

Schütt, K. T., Kindermans, P., Sauceda, H., Chmiela, S., Tkatchenko, A., & Müller, K. (2017). SchNet: A continuous-filter convolutional neural network for modeling quantum interactions..

Senftle, T. P., Hong, S., Islam, M. M., Kylasa, S. B., Zheng, Y., Shin, Y. K., . . . van Duin, A. C. T. (2016). The ReaxFF reactive force-field: development, applications and future directions. *NPJ Comp. Mater.*, *2*.

Senn, H. M., & Thiel, W. (2009). QM/MM Methods for Biomolecular Systems. *Angew. Chem. Intern. Ed.*, *48*(7), 1198-1229.

Siegbahn, P. E. M., Blomberg, M. R. A., & Chen, S.-L. (2010). Significant van der Waals

Effects in Transition Metal Complexes. *J. Chem. Theo. Comp.*, *6*(7), 2040-2044.

Silatani, M., Lima, F. A., Penfold, T. J., Rittman, J., Reinhard, M., Rittmann-Frank, H., . . . Chergui, M. (2015). NO binding kinetics in Myoglobin investigated by picosecond Fe K-edge absorption spectroscopy. *Proc. Natl. Acad. Sci.*, *112*(), 12922 - 12927.

Skokov, S., Peterson, K. A., & Bowman, J. M. (1998). An Accurate Ab Initio HOCl Potential Energy Surface, Vibrational and Rotational Calculations, and Comparison with Experiment. *J. Chem. Phys.*, *109*(7), 2662–2671.

Skouteris, D., Castillo, J., & Manolopoulos, D. (2000). ABC: a quantum reactive scattering program. *Comput. Phys. Commun.*, *133*(1), 128-135.

Soloviov, M., Das, A. K., & Meuwly, M. (2016). Structural Interpretation of Metastable States in Myoglobin-NO. *Angew. Chem. Intern. Ed.*, *55*(34), 10126-10130.

Soloviov, M., & Meuwly, M. (2014). CO-dynamics in the active site of cytochrome c oxidase. *J. Chem. Phys.*, *140*(14).

Soloviov, M., & Meuwly, M. (2015). Reproducing kernel potential energy surfaces in biomolecular simulations: Nitric oxide binding to myoglobin. *J. Chem. Phys.*, *143*(10).

Sorbie, K. S., & Murrell, J. N. (1975). Analytical Potentials for Triatomic Molecules from Spectroscopic Data. *Mol. Phys.*, *29*(5), 1387-1407.

Storn, R., & Price, K. (1997). Differential evolution–a simple and efficient heuristic for global optimization over continuous spaces. *J. Global Optim.*, *11*(4), 341–359.

Strachan, A., van Duin, A. C. T., Chakraborty, D., Dasgupta, S., & Goddard III, W. A. (2003). Shock waves in high-energy materials: The initial chemical events in nitramine RDX. *Phys. Rev. Lett.*, *91*, 098301-1.

Strajbl, M., Hong, G., & Warshel, A. (2002). Ab initio QM/MM simulation with proper sampling: "First principle" calculations of the free energy of the autodissociation of water in aqueous solution. *J. Phys. Chem. B*, *106*, 13333-13343.

Sumpter, B. G., & Noid, D. W. (1992). Potential energy surfaces for macromolecules. a neural network technique. *Chem. Phys. Lett.*, *192*(5), 455–462.

Szymczak, J. J., Hofmann, F. D., & Meuwly, M. (2013). Structure and dynamics of solvent shells around photoexcited metal complexes. *Phys. Chem. Chem. Phys.*, *15*(17), 6268-6277.

Tinajero-Trejo, M., Denby, K. J., Sedelnikova, S. E., Hassoubah, S. A., Mann, B. E., & Poole, R. K. (2014). Carbon Monoxide-releasing Molecule-3 (CORM-3; $Ru(CO)_3Cl(Glycinate)$) as a Tool to Study the Concerted Effects of Carbon Monoxide and Nitric Oxide on Bacterial Flavohemoglobin Hmp: Applications and pitfalls. *J. Biol. Chem.*, *289*(43), 29471-29482.

Tong, X., Nagy, T., Reyes, J. Y., Germann, M., Meuwly, M., & Willitsch, S. (2012). State-selected ion-molecule reactions with coulomb-crystallized molecular ions in traps. *Chem. Phys. Lett.*, *547*, 1-8.

Traylor, T., & Sharma, V. (1992). Why NO. *Biochem.*, *31*(11), 2847-2849.

Tubert-Brohman, I., Schmid, M., & Meuwly, M. (2009). A molecular mechanics force field for octahedral organometallic compounds with inclusion of the trans influence. *J. Chem. Theo. Comp.*, *5*, 530.

Unke, O. T., Castro-Palacio, J. C., Bemish, R. J., & Meuwly, M. (2016). Collision-Induced Rotational Excitation in N^{2+} ($^2\Sigma_g^+$, $\nu = 0$)–Ar: Comparison of Computations and Experiment. *J. Chem. Phys.*, *144*(22), 224307.

Unke, O. T., & Meuwly, M. (2017). Toolkit for the Construction of Reproducing Kernel-Based Representations of Data: Application to Multidimensional Potential Energy Surfaces. *J. Chem. Inf. Model.*, *57*(8), 1923-1931.

Unke, O. T., & Meuwly, M. (2018). A Reactive, Scalable and Transferable Model for Molecular Energies from a Neural Network Approach Based on Local Information. *J. Chem. Phys.*, *148*.

Vaida, V., & Donaldson, D. J. (2014). Red-light initiated atmospheric reactions of vibrationally excited molecules. *Phys. Chem. Chem. Phys.*, *16*, 827-836.

Vaida, V., Kjaergaard, H. G., Hintze, P. E., & Donaldson, D. J. (2003). Photolysis of sulfuric acid vapor by visible solar radiation. *Science*, *299*(5612), 1566 - 1568.

Valero, R., Song, L., Gao, J., & Truhlar, D. G. (2009a). Erratum: Perspective on Diabatic Models of chemical reactivity as illustrated by the gas-phase S_N2 reaction of acetat ion with 1,2-Dichloroethane. *J. Chem. Theo. Comp.*, *5*, 2191-2191.

Valero, R., Song, L., Gao, J., & Truhlar, D. G. (2009b). Perspective on Diabatic Models of chemical reactivity as illustrated by the gas-phase S_N2 reaction of acetat ion with

1,2-Dichloroethane. *J. Chem. Theo. Comp.*, *5*, 1-22.

Valli, G., Orru, R., Clementi, E., Lagana, A., & Cro cchianti, S. (1995). Rate coefficients for the N+O$_2$ reaction computed on an ab initio potential energy surface. *J. Chem. Phys.*, *102*, 2825-2832.

van Duin, A. C. T., Dasgupta, S., Lorant, F., & Goddard III, W. A. (2001). ReaxFF: A Reactive Force field for hydrocarbons. *J. Phys. Chem. A*, *105*, 9396-9409.

van der Avoird, A., Pedersen, T. B., Dhont, G. S. F., Fernandez, B., & Koch, H. (2006). Ab initio potential-energy surface and rovibrational states of the HCN-HCl complex. *J. Chem. Phys.*, *124*(20).

van der Kamp, M. W., & Mulholland, A. J. (2013). Combined Quantum Mechanics/Molecular Mechanics (QM/MM) Methods in Computational Enzymology. *Biochem.*, *52*(16), 2708-2728.

Varandas, A. (2003). A realistic multi-sheeted potential energy surface for NO$_2$(^{2}A') from the double many-body expansion method and a novel multiple energy-switching scheme. *J. Chem. Phys.*, *119*(5), 2596-2613.

Vashishta, P., Kalia, R. K., & Nakano, A. (2006). Multimillion atom simulations of dynamics of oxidation of an a luminum nanoparticle and nanoindentation on ceramics. *J. Phys. Chem. B*, *110*, 3727-3733.

Vendrell, O., Gatti, F., & Meyer, H.-D. (2007). Dynamics and infrared spectroscopy of the protonated water dimer. *Angew. Chem. Intern. Ed.*, *46*(36), 6918-6921.

Vendrell, O., Gatti, F., & Meyer, H.-D. (2009). Full dimensional (15 dimensional) quantum-dynamical simulation of the protonated water-dimer IV: Isotope effects in the infrared spectra of D(D$_2$O)$_2^+$, H(D$_2$O)$_2^+$, and D(H$_2$O)$_2^+$ isotopologues. *J. Chem. Phys.*, *131*(3).

Voth, G. (2006). Computer simulation of proton solvation and transport in aqueous and biomolecular systems. *Acc. Chem. Res.*, *39*(2), 143-150.

Wang, L.-P., Titov, A., McGibbon, R., Liu, F., Pande, V. S., & Martinez, T. J. (2014). Discovering chemistry with an ab initio nanoreactor. *Nat. Chem. Biol.*, *6*(12), 1044-1048.

Warshel, A. (1984). Dynamics of enzymatic reactions. *Proc. Natl. Acad. Sci.*, *81*, 444-448.

Warshel, A., Chu, Z. T., Villa, J., Strajbl, M., Schutz, C. N., Shurki, A., ... Schopf, P.

(2012). Molaris-xg, v 9.11 [Computer software manual].

Warshel, A., & Weiss, R. M. (1980). An empirical valence bond approach for comparing reactions in solutions and in enzymes. *J. Am. Chem. Soc.*, *102*, 6218-6226.

Weinert, H. L. (1982). *Reproducing kernel hilbert spaces: Applications in statistical signal processing* (Vol. 25). Hutchinson Ross Pub. Co. London.

White, C. A., Johnson, B. G., Gill, P. M., & Head-Gordon, M. (1996). Linear scaling density functional calculations via the continuous fast multipole method. *Chem. Phys. Lett.*, *253*(3), 268–278.

Wiedemair, M. J., Hitzenberger, M., & Hofer, T. S. (2015). Tuning the reactivity of a dissociative force field: proton transfer properties of aqueous H_3O^+ and their dependence on the three-body interaction. *Phys. Chem. Chem. Phys.*, *17*(16), 10934-10943.

Wolf, M. G., & Groenhof, G. (2014). Explicit Proton Transfer in Classical Molecular Dynamics Simulations. *J. Comput. Chem.*, *35*(8), 657-671.

Worner, H. J., Arrell, C. A., Banerji, N., Cannizzo, A., Chergui, M., Das, A. K., . . . Wenger, O. (2017). Charge migration and charge transfer in molecular systems. *Struct. Dyn.*, *4*(6).

Wrenn, S. J., Butler, L. J., Rowland, G. A., Knox, C. J., & Phillips, L. F. (1999). The necessity for multiphoton processes in the 193-nm photochemistry of sulphuric acid aerosols. *J. Chem. Phys.*, *129*(3), 1112 - 1118.

Xu, Z.-H., & Meuwly, M. (2017). Vibrational Spectroscopy and Proton Transfer Dynamics in Protonated Oxalate. *J. Phys. Chem. A*, *121*(29), 5389-5398.

Xu, Z.-H., & Meuwly, M. (2018). Multi-state reactive molecular dynamics simulations of proton diffusion in water clusters and in bulk. *J. Chem. Theo. Comp.*, *submitted*.

Yang, Y., & Meuwly, M. (2010). A generalized reactive force field for nonlinear hydrogen bonds: Hydrogen dynamics and transfer in malonaldehyde. *J. Chem. Phys.*, *133*(6).

Yoo, B.-K., Kruglik, S. G., Lamarre, I., Martin, J.-L., & Negrerie, M. (2012). Absorption Band III Kinetics Probe the Picosecond Heme Iron Motion Triggered by Nitric Oxide Binding to Hemoglobin and Myoglobin. *J. Phys. Chem. B*, *116*(13), 4106-4114.

Yosa, J., & Meuwly, M. (2011). Vibrationally Induced Dissociation of Sulfuric Acid (H_2SO_4). *J. Phys. Chem. A*, *115*(50), 14350 - 14360.

Yosa Reyes, J., Brickel, S., Unke, O. T., Nagy, T., & Meuwly, M. (2016). HSO$_3$Cl: a prototype molecule for studying OH-stretching overtone induced photodissociation. *Phys. Chem. Chem. Phys.*, *18*(9), 6780-6788.

Yosa Reyes, J., Nagy, T., & Meuwly, M. (2014). Competitive Reaction Pathways in Vibrationally Induced Photodissociation of H$_2$SO$_4$. *Phys. Chem. Chem. Phys.*, *16*, 18533-18544.

Zeldovich, Y. (1946). The Oxidation of Nitrogen in Combustion Explosions. *Acta Physicochimica U.S.S.R.*, *21*(), 577-628.

Zhang, W., Zhou, Y., Wu, G., Lu, Y., Pan, H., Fu, B., . . . Yang, X. (2010). Depression of reactivity by the collision energy in the single barrier H + CD$_4$ → HD + CD$_3$ reaction. *Proc. Natl. Acad. Sci.*, *107*(29), 12782-12785.

Zhang, X., Braams, B. J., & Bowman, J. M. (2006). An Ab Initio Potential Surface Describing Abstraction and Exchange for H + CH$_4$. *J. Chem. Phys.*, *124*(2), 021104.

Zhao, Z., Zhang, Z., Liu, S., & Zhang, D. H. (2017). Dynamical barrier and isotope effects in the simplest substitution reaction via Walden inversion mechanism. *Nat. Comm.*, *8*.